

Review

Brief Review of Photocatalysis and Photoresponse Properties of ZnO–Graphene Nanocomposites

Chenhao Gao ^{1,†}, Keyi Zhong ^{2,†}, Xuan Fang ^{1,2,*}, Dan Fang ^{1,*}, Hongbin Zhao ^{3,*}, Dengkui Wang ¹, Bobo Li ⁴, Yingjiao Zhai ¹, Xueying Chu ¹, Jinhua Li ¹ and Xiaohua Wang ¹

- ¹ State Key Laboratory of High Power Semiconductor Lasers, School of Science, Changchun University of Science and Technology, Changchun 130022, China; 2019100136@mails.cust.edu.cn (C.G.); wangdk@cust.edu.cn (D.W.); yjzhai@cust.edu.cn (Y.Z.); xueying_chu@cust.edu.cn (X.C.); lijh@cust.edu.cn (J.L.); biewang2001@126.com (X.W.)
 - ² School of Science and Engineering, The Chinese University of Hong Kong, Shenzhen 518172, China; 2021100149@mails.cust.edu.cn
 - ³ State Key Laboratory of Advanced Materials for Smart Sensing, General Research Institute for Nonferrous Metals, Beijing 100088, China
 - ⁴ College of New Materials and New Energies, Shenzhen Technology University, Shenzhen 518118, China; libobo@sztu.edu.cn
- * Correspondence: fangx@cust.edu.cn (X.F.); fangdan@cust.edu.cn (D.F.); zhaohongbin@grinm.com (H.Z.)
† Chenhao Gao and Keyi Zhong contributed equally to this work.

Abstract: As a typical wide bandgap semiconductor, ZnO has received a great deal of attention from researchers because of its strong physicochemical characteristics. During the past few years, great progress has been made in the optoelectronic applications of ZnO, particularly in the photocatalysis and photodetection fields. To enable further improvements in the material's optoelectronic performance, construction of a variety of ZnO-based composite structures will be essential. In this paper, we review recent progress in the growth of different ZnO–graphene nanocomposite structures. The related band structures and photocatalysis and photoresponse properties of these nanocomposites are discussed. Additionally, specific examples of the materials are included to provide an insight into the common general physical properties and carrier transport characteristics involved in these unique nanocomposite structures. Finally, further directions for the development of ZnO–graphene nanocomposite materials are forecasted.

Keywords: ZnO–graphene nanocomposite; photocatalysis; photoresponse



Citation: Gao, C.; Zhong, K.; Fang, X.; Fang, D.; Zhao, H.; Wang, D.; Li, B.; Zhai, Y.; Chu, X.; Li, J.; et al. Brief Review of Photocatalysis and Photoresponse Properties of ZnO–Graphene Nanocomposites. *Energies* **2021**, *14*, 6403. <https://doi.org/10.3390/en14196403>

Academic Editor: Abdul-Ghani Olabi

Received: 30 August 2021

Accepted: 28 September 2021

Published: 7 October 2021

Publisher's Note: MDPI stays neutral with regard to jurisdictional claims in published maps and institutional affiliations.



Copyright: © 2021 by the authors. Licensee MDPI, Basel, Switzerland. This article is an open access article distributed under the terms and conditions of the Creative Commons Attribution (CC BY) license (<https://creativecommons.org/licenses/by/4.0/>).

1. Introduction

With its large direct bandgap (3.37 eV) and high exciton binding energy (60 meV), crystalline ZnO is recognized as a good material for optoelectronics applications, including photodetectors [1–3], light-emitting diodes [4–6], nanogenerators [7,8], and solar cells [9,10]. In addition, because of its stability, nontoxicity, and biocompatibility, ZnO can be used in chemical and biomedical applications, including gas sensors [11,12], Parkinson's disease detection [13], and cancer diagnostics [14].

The material's large direct band gap means that ZnO can not only absorb photons easily, with no need for a momentum change but can also absorb photons with high energy. A high surface-to-volume ratio is beneficial for high absorption efficiency. Additionally, the ZnO electron mobility is almost double that of TiO₂, which means that recombination can be inhibited much more easily in ZnO [15]. Furthermore, ZnO is low in cost, environmentally friendly [2], abundant [16], and easy to synthesize [17]. These characteristics make ZnO a practical and sustainable photocatalytic material and have drawn much attraction in optoelectronics fields.

However, the direct bandgap of ZnO also leads to problems, including high recombination rates and reduced efficiency. In addition, agglomeration [18] and photocorrosion [19]

limit the performance and the lifetime of ZnO. In recent years, many researchers have effectively optimized the properties of materials through the construction of nanocomposites [20,21]. Establishment of appropriate nanocomposites can also solve the problems of ZnO [22–26]. In this approach, the nanocomposite formation through coupling using a narrow band gap semiconductor has been proved as potential strategy to enhance the lifetime of photoinduced charge carriers by effective charge separation [27]. The efficient electron and hole transfer from the conduction band and valence band of ZnO, respectively, at the interface have proved to enhance the corrosion resistance of ZnO during photocatalytic reactions [28]. These drawbacks can be offset by combining ZnO with graphene, which has a large surface area, high carrier mobility [29], excellent light transparency, beneficial flexibility [16], and good chemical and mechanical stability [2]. When ZnO makes contact with graphene, the work function of graphene is lower than the ZnO conduction band [30]. Therefore, electrons that are excited to the ZnO conduction band move to graphene and thus inhibit recombination in ZnO. The large surface area and high carrier mobility of graphene both contribute to its high efficiency, while graphene's transparency ensures that photons can arrive at the ZnO location and thus be used as much as possible. Finally, embedding ZnO on graphene can also prevent both materials from aggregating to maintain their high surface-to-volume ratio and thus their excellent efficiency [31].

Because of the synergistic effect of combining ZnO with graphene, ZnO–graphene composites have good prospects for application to photocatalysis and photodetection. Figure 1 shows an application diagram for ZnO–graphene materials with different structures. In this work, we present a brief review of the development of ZnO–graphene composites from four perspectives: the different structures of the ZnO–graphene composites and their use in photocatalysis, photodetection, and other applications.

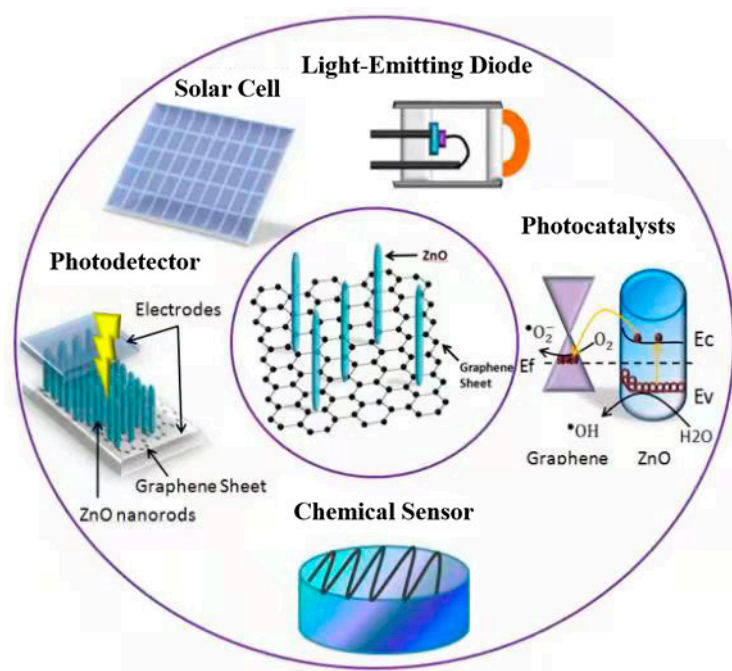


Figure 1. Application and development of ZnO–graphene nanocomposite structures.

2. The Principles of Photocatalytic and Photoresponse Properties of Nanocomposites

2.1. The Photocatalytic Principles of ZnO and Related Nanocomposites

Normally, the mainly photocatalytic reaction processes of ZnO are as follows: (a) absorption of photons to form electron–hole pairs, (b) the separation and migration of photogenerated carriers, (c) the redox reactions between photogenerated carriers and degraded materials absorbed on the surface of ZnO, and (d) decomposition process of degraded materials. Although ZnO can only absorb high energy of incident light, we can still enhance photocat-

alytic properties by improving the transfer processes of photogenerated carriers. Taking ZnO–graphene composite materials as an example, the mechanism of photocatalytic activity of the G–ZnO–Au composite is shown in Figure 2. UV light can generate a large number of free electrons in the conduction band and holes in the valence band. The valence and conduction bands of ZnO have work functions of -7.25 and -4.05 eV (vs. vacuum), and because of the large work functions of graphene (about -4.42 eV), type II band alignment is formed. Therefore, the electrons transfer rapidly from ZnO to graphene, which can reduce h^+/e^- recombination greatly. Thus it can be seen that ZnO–graphene nanocomposite structure has great potential for transferring photogenic carriers.

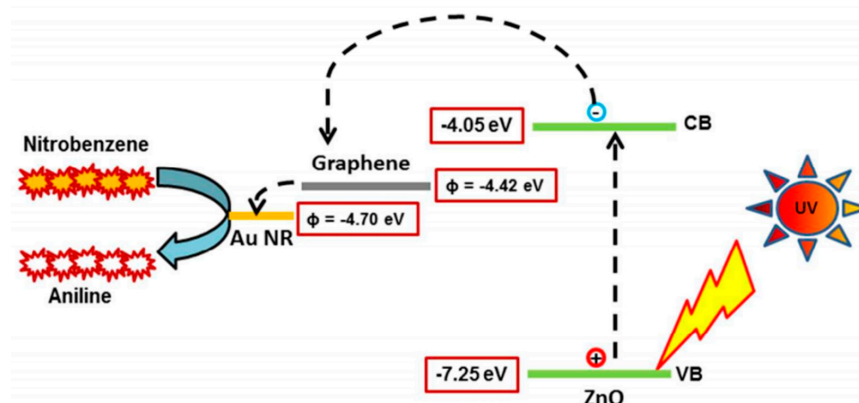
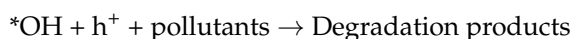
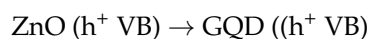
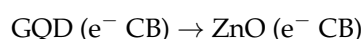
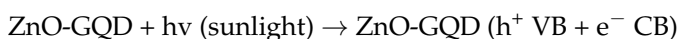


Figure 2. Schematic illustration of energy band diagram and a proposed mechanism of the charge carrier transitions in G–ZnO–Au composite towards photocatalytic nitrobenzene degradation under UV light irradiation.

In addition, with downsizing the dimension from two dimensions to zero dimensions, a band gap can be introduced for nanostructured graphene due to quantum confinement and edge effects. This makes the electron–hole separation ability of these types of ZnO–graphene composite more interesting. The entire photocatalytic reaction mechanism is proposed by Suneel Kumar [32] as follows:



A schematic illustration of energy band diagram and a proposed mechanism of the charge carrier transitions in ZnO–graphene quantum dot (GQD) composite towards photocatalytic pollutant degradation is as follows in Figure 3. The strong interfacial contact between ZnO and GQD leads to the transfer of photoexcited electrons from the more negative CB of ZnO. The photoinduced holes move up-potential from VB of ZnO to VB of GQD, which triggers the photoinduced electron–hole separation efficiently across the composites.

2.2. The Photoresponse Principles of ZnO and Related Nanocomposites

Due to high photoconductive gain property, ZnO and its nanostructures are exhibiting potential in photodetection applications. The photoconductive mechanism is mainly a result of two factors: (1) large surface-to-volume ratio and the presence of deep level surface trap states, which enable enough high energy photons to be absorbed and prolong the photocarrier lifetime, and (2) the reduced dimensionality can shorten the carrier

transit time and increase carrier collection efficiency. In C. Soci's work [33] shown in Figure 4a–c, a physical model that illustrates the origin of the photoconductive gain in the ZnO nanostructure is presented, indicating that oxygen adsorption and desorption occur at the ZnO surface, then photogenerated holes are trapped by the presence of oxygen-related hole-trap states, which prevents photogenerated carrier recombination. These photocarrier relaxation dynamics are almost the same as the photocatalytic principles of semiconductors, which means that improving photogenerated carrier transport process could also enhance photoresponse performance, as shown in Figure 4e. In the ZnO–graphene heterojunction, photogenerated holes migrate to the surface and are captured by oxygen adsorption, then the remaining unpaired electrons in the conduction band of the ZnO transfer to the graphene layer [34]. With the advantage of high mobility of graphene, the transferred electrons are collected by electrodes. Therefore, the ZnO–graphene heterojunction can not only enhance photoresponse ability but also increase photoresponse time.

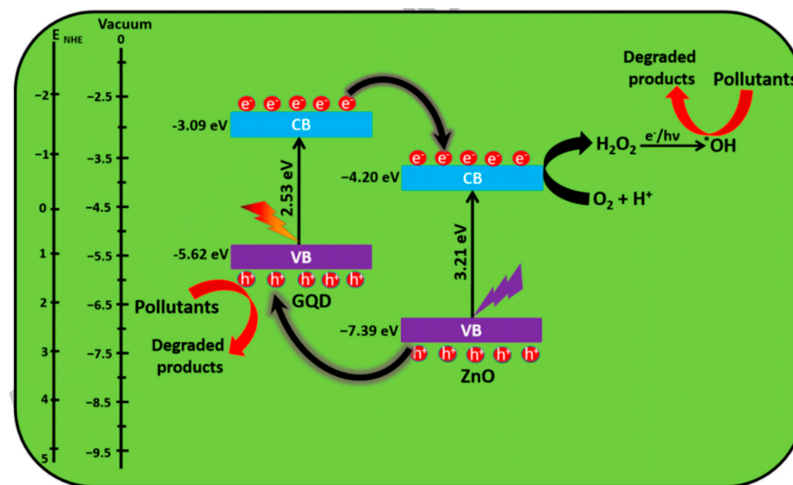


Figure 3. Schematic illustration of energy band diagram and a proposed mechanism of the charge carrier transitions in ZnO–GQD composite towards photocatalytic pollutant degradation under natural sunlight irradiation.

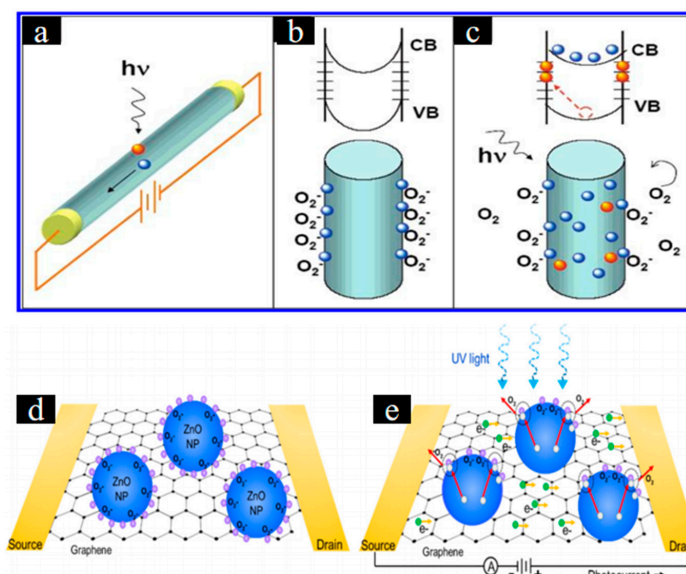


Figure 4. (a–c) Photoconduction in ZnO nanowire (NW) photodetectors. (a) Schematic of a ZnO NW photoconductor. (b,c) Schematic of trapping and photoconduction mechanism in ZnO NWs (a) in the dark and (b) under UV illumination. Schematic of photoconduction mechanism for ZnO nanoparticle–graphene photodetectors (d) without and (e) with UV illumination (not to scale).

3. Synthesis and Structural Characteristics of ZnO–Graphene Composites

Graphene has three morphologies: zero-dimensional (0D) graphene quantum dots (GQDs), two-dimensional (2D) graphene sheets, and three-dimensional (3D) graphene foam. Therefore, ZnO–graphene composites can be divided into three classes based on these morphologies. The first type is the ZnO–0D GQD composite, which is made by embedding small graphene nanoparticles with diameters ranging from 3 to 35 nm on the surface of a ZnO crystal. The second type is synthesized by inlaying ZnO crystals on a 2D graphene sheet. In the third type of composite, ZnO crystals are grown on a 3D graphene foam, which consists of a graphene sheet network. The different structures of each of these three composite types are discussed in this section.

3.1. ZnO–0D Graphene Quantum Dot Composite

Multiple methods are available to fabricate quantum dots (QDs) easily and cost-effectively. In addition, QDs are well developed for use in high-sensitivity applications because of their high photostability and brightness. Therefore, researchers have studied QDs in great depth for a number of years. In 2015, Wang et al. [35] synthesized Ag nanoparticle–GQD–ZnO flower ternary composites for use in photocatalysis applications. The Ag nanoparticles can enhance the light absorption ability of the materials, but the contact between the 2–5 nm GQDs and ZnO is affected seriously by the 28 nm Ag nanoparticles. Therefore, the advantages of the GQD–ZnO composites were not exploited in this case.

To increase the contact area between the GQDs and ZnO and thus improve the material properties, many researchers have investigated composites composed of GQDs and ZnO nanowires (nanorods). In addition, they produced different composite materials and application fields by adjusting the sizes of and the growth methods for both the GQDs and the ZnO nanowires (nanorods). At present, the composites based on ZnO nanowires still have good development and broad application prospects [36]. Dhar et al. [37] deposited GQDs with a size of approximately 6 nm on the surfaces of ZnO nanorods with a diameter of 100 nm for ultraviolet (UV) light detection in 2016. The structural diagram and a simple energy band diagram are shown in Figure 5a. The materials all have a high specific surface area and thus form excellent composite contacts. However, the GQD content obtained by the dipping process is uncertain, and the method takes a long time and wastes the GQD solution. In 2016, Ebrahimi et al. [38] synthesized ZnO nanowire–GQD composites in a convenient, fast, and low-cost manner for photocatalysis applications. GQDs with a size of approximately 17 nm and ZnO nanowires with diameters of 170–250 nm were first grown using an electrochemical method and an anodization process, respectively. With diameters in the 170–250 nm range, these ZnO nanowires have a low surface-to-volume ratio, but they have good development prospects in photocatalysis applications.

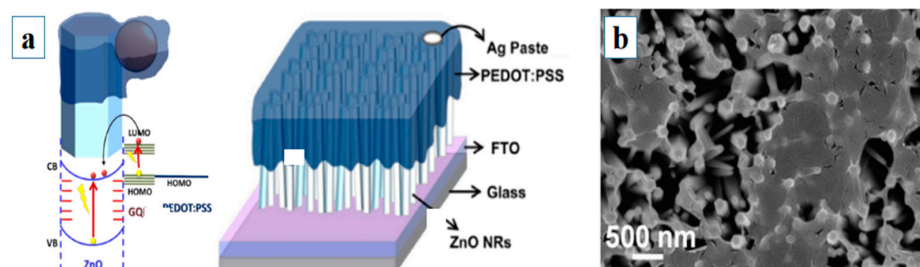


Figure 5. (a) Flow-process diagram for Ag nanoparticle–graphene quantum dot (GQD)–ZnO flower composite fabrication; (b) Schematic representation of ZnO nanorod (NR)/PEDOT:PSS polymer Schottky diode.

Ghosh et al. [39] also explored different fabrication methods and material sizes for composites based on GQDs and ZnO nanowires (nanorods). Ghosh's group fabricated ZnO nanorod–GQD composites consisting of ZnO nanorods with diameters of approximately 500 nm and GQDs with sizes of around 3 nm for photodetection applications in 2016.

The ZnO nanorods were first grown using a methanol-assisted hydrothermal method, and the GQDs were prepared via high pressure microwave irradiation of citric acid and ethanolamine. After that, an aqueous solution of the GQDs was spin coated on the ZnO nanorods. Figure 5b shows an FFSEM image of rGO deposited on ZnO nanorod array. The method of Ghosh et al. is suitable for production of ZnO–GQD composites.

Inclusion of metals would be beneficial for both the recombination rate and the light absorption of these materials. Therefore, metals were added to the ZnO nanorod–GQD composites to achieve higher light absorption [40,41]. This method not only formed ZnO–GQD composites to reduce the recombination rate but also enhanced the light absorption.

3.2. ZnO–2D Graphene Composites

Because the research into this type of material is very extensive, the development of these composites is explained from three perspectives, involving changing the material structure, use of doping, and using a combination of structural change and material doping. Finally, the devices fabricated using this material type are summarized.

3.2.1. Changing the ZnO–2D Graphene Structure

One method that is used to change the properties of materials is to change the material structure; this approach is commonly used in composites in particular. Because of the extensive existing research into changing the structure of ZnO–2D graphene sheets, the resulting composites are classified and summarized based on the structural changes in ZnO. In this section, the ZnO structures are divided into nanoparticles, nanowires (nanorods), and nanosheets.

The sizes, distributions, and contact modes of the ZnO nanoparticles have different effects on the composites, and this has also attracted the interest of many researchers. Wu et al. [42] stated that stability has always been an important aspect of photocatalysis and related devices, and that this also applies for ZnO–2D graphene sheets. In 2009, Wu's group synthesized sandwich-like ZnO nanoparticle–graphene sheet–ZnO nanoparticle composites with a structure that not only protected the graphene from air oxidation but also increased the composite's thermal stability and UV absorption. Unlike the traditional ZnO–2D graphene sheet structures, Wu et al. used sandwich structures to enhance the properties of their materials.

Bu et al. [15] also used ZnO nanoparticle–2D graphene composites in their research. Interestingly, while other researchers changed the structures and the dopant materials to improve the properties of their composites, Bu et al. [15] changed the number of layers of graphene in their structures. In 2013, they synthesized graphene–ZnO quasi-shell–core hybrid composites by using two to three layers of rGO sheets to cover an aggregate of ZnO nanoparticles with diameters of approximately 500 nm for photocatalysis applications. A scanning electron microscope (SEM) image of the resulting graphene–ZnO quasi-shell–core structure is shown in Figure 6a. In recent years, ZnO nanoparticle–2D graphene sheet structures have been investigated intensively. However, these ZnO nanoparticles have generally only been located on the surface of the 2D graphene sheet. However, Ezeigwe et al. [16] embedded ZnO nanoparticles with diameters of 200 nm in a graphene sheet to improve its capacitive performance and the average energy density of its superconductivity in 2014. First, graphene flakes were obtained by sonicating graphite in a mixture of ethanol and water. Then, zinc nitrate hexahydrate was added to this graphene flake solution to grow ZnO nanoparticles via the solvothermal synthesis method in an environment with a pH of 12. SEM images of the materials obtained are shown in Figure 6b,c.

With regard to structural change in ZnO nanoparticle–2D graphene composites, the research of Xu et al. [18] is highly innovative. They modified ZnO nanoparticles into ZnO flower structures and subsequently compounded micro-sized ZnO flower–rGO composite for photodegradation applications in 2014. The idea of adjusting the concentrations in the reaction solution has been used widely in the development of materials. Khoa et al. [40] decorated ZnO–rGO hollow microspheres in 2014 for photocatalysis applications. Addition-

ally, Bera et al. [17] acknowledged that continued development of ZnO–graphene hollow microsphere structures would offer exciting opportunities to produce high-performance devices. In 2015, they used a low-temperature solution method to synthesize hierarchically structured ZnO–graphene sheet hollow microspheres with diameters of approximately 50 nm. The performance of these composites in degrading rhodamine B dye was better than that of a commercially available photocatalytic chemical product, P25 (a type of degradation catalyst) (TiO_2). During their process, ZnO–graphene sheet core-shell structured nanoparticles with sizes of approximately 12 nm first aggregated and then underwent further Ostwald ripening. When the graphene oxide to zinc acetate dihydrate weight ratio was 0.032, the composites exhibited the optimal photocatalysis performance. The ZnO–graphene hollow microsphere structure growth process is illustrated in Figure 6d.

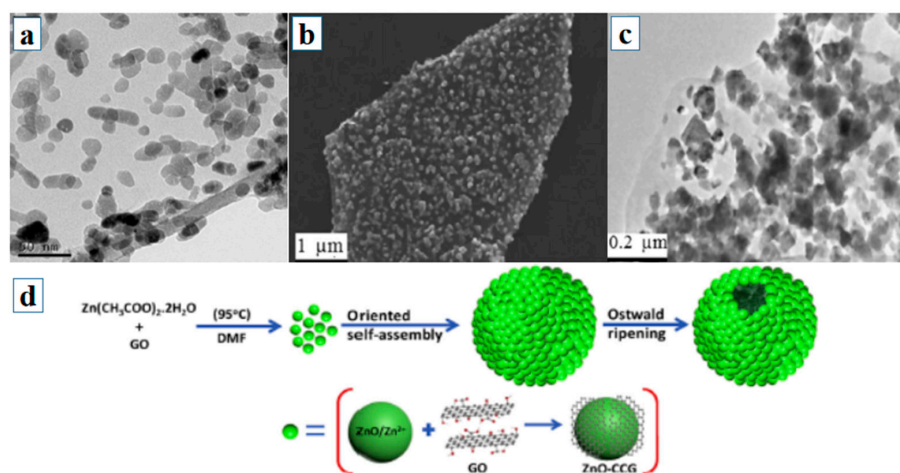


Figure 6. (a) Scanning electron microscope (SEM) image of graphene–ZnO quasi-shell–core structure; (b,c) SEM images of embedded ZnO nanoparticle–graphene sheet composites; (d) growth process of the ZnO–graphene hollow microsphere structure.

In 2013, Xu et al. [43] also explored the idea of varying the number of layers of graphene in a manner similar to Bu et al. For their study of ZnO nanowire–2D graphene composites, Xu et al. optimized the number of graphene layers and the positions and arrangement of the nanowires. They aligned ZnO nanowires with diameters of approximately 45 nm vertically on bilayer graphene sheets for photodetection applications. The bilayer graphene sheet was first synthesized by chemical vapor deposition (CVD) and then moved onto a p-type silicon substrate with a 300 nm-thick SiO_2 layer. ZnO nanowires were then grown on the graphene layer using a hydrothermal approach. It should be noted here that vertically aligned nanowires were first combined with bilayer graphene sheets by Xu et al. Their findings provided a viable source material for fabrication of lasers and detectors. Influenced by the sandwich structure of Wu et al., Boruah et al. [44] synthesized sandwich-structured graphene–ZnO nanowire–graphene hybrids for UV detection applications in 2015. A graphene layer was first grown on a copper substrate via atmospheric CVD and then transferred onto a SiO_2/Si substrate. ZnO nanowires with diameters of 20–40 nm were subsequently grown on the graphene layer with the resistive thermal evaporation method. Poly (bisphenol carbonate) (PC)-coated graphene was then transferred onto the other side of the ZnO nanowires.

3.2.2. ZnO–2D-Graphene-Doped Substances

The structures of the ZnO–2D-graphene-doped substances are explained from three material perspectives, involving nanoparticles, nanorods, and nanotubes. There are many ways to improve the properties of materials, e.g., through addition of metals, compounds, and carbon nanotubes. Therefore, different ZnO structures and dopant materials can provide various advantages.

Roy et al. [45] acknowledged the idea of adding substances to improve the properties of existing materials and they inlaid ZnO nanoparticles with diameters of 45.3 ± 3.7 nm and Au nanorods with diameters of approximately 14.1 ± 1.3 nm into graphene sheets to increase the efficiency of photocatalysis in 2013. After preparing the seed and the growth solution, Au nanorods were fabricated via a seed mediated method. Subsequently, the prepared Au nanorods and the graphene oxide solution were added to a precursor solution consisting of zinc acetate, and the mixture finally underwent a simple one-pot hydrothermal process. An SEM image of the ZnO nanoparticle–Au nanorod–graphene sheet structure is shown in Figure 7a.

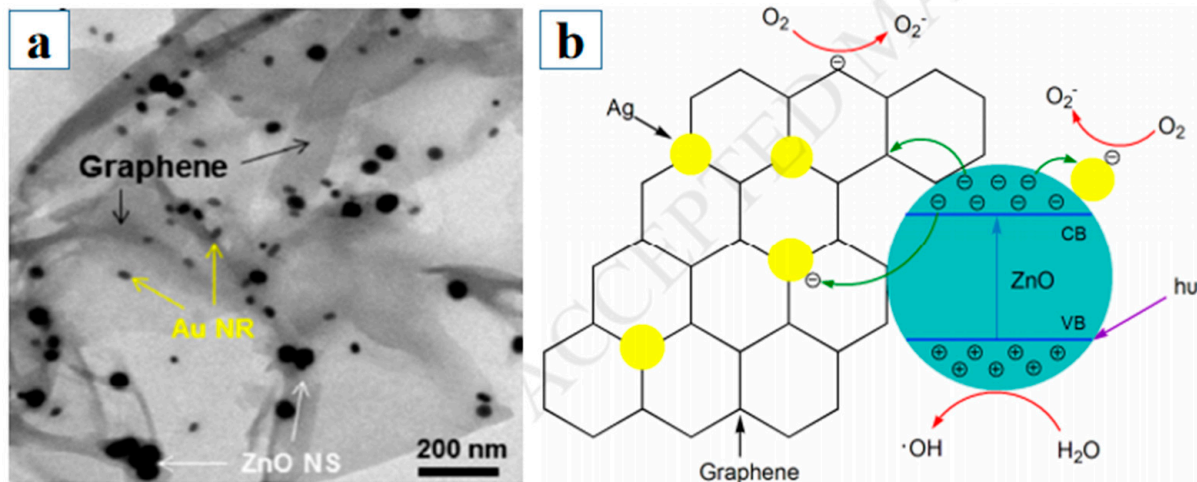


Figure 7. (a) SEM image of ZnO nanoparticle–Au nanorod (NR)–graphene sheet; (b) structural schematic diagram of the photocatalytic reduction of Ag/ZnO/Graphene nanocomposites.

With regard to the nanorods and nanotubes, metals, compounds, and carbon nanotubes can be used for doping. In 2012, Lv et al. [41] embedded ZnO nanorods into 2D rGO sheets with carbon nanotubes wound between them for photocatalysis applications. The diameters of the ZnO nanorods and carbon nanotubes ranged from 40 to 60 nm. Their experiments focused on the ZnO to rGO weight ratio, which was 89.9:1. For the synthesis process, a graphite oxide suspension and carbon nanotubes were first added to a $\text{Zn}(\text{NO}_3)_2$ solution, and the pH value of the mixture was adjusted to within the range 10–11 by adding a NaOH solution. The mixture was then placed into an automated focused microwave system to form the ZnO nanorod–rGO sheet–carbon nanotube composites.

To improve the properties of the ZnO nanorods, Han et al. [19] decorated rGO with an array of CdS-sensitized ZnO nanorods for visible light photocatalysis in 2014. To synthesize these structures, graphene oxide was first dispersed in a ZnO seed solution composed of a mixture of zinc acetate dihydrate solution and KOH solution in methanol. The precipitate obtained was then dispersed in an aqueous $\text{Zn}(\text{NO}_3)_2$ and $\text{C}_6\text{H}_{12}\text{N}_4$ solution. After the solution was refluxed, ZnO nanorod–rGO nanocomposites were formed and were then dispersed in deionized water. This nanocomposite suspension was combined with $\text{CdSO}_4 \cdot 8/3\text{H}_2\text{O}$ and NH_2CSNH_2 , and the resulting solution underwent a refluxing process.

In 2014, Dou et al. [46] fabricated Ag nanoparticle–ZnO NR–2D graphene photocatalysts. When compared with the composites of Roy et al., they replaced the ZnO nanoparticles with Ag nanoparticles and the Au NRs with ZnO NRs. To synthesize their structures, pre-prepared graphite oxide was first dispersed in water and subjected to ultrasonication. Subsequently, $\text{Zn}(\text{NO}_3)_2 \cdot 6\text{H}_2\text{O}$, AgNO_3 , and $\text{C}_6\text{H}_{12}\text{N}_4$ were added to the dispersion, and the mixture was finally placed into an ultrasonic microwave reaction system to grow the ZnO NRs and Ag nanoparticles. A structural schematic diagram of the photocatalytic reduction of Ag/ZnO/Graphene nanocomposites is shown in Figure 7b.

3.2.3. ZnO–2D Graphene with Both Structural Change and Doping

After introducing the methods of using either structural changes or doping to improve the composite material properties, the composite materials produced using a combination of structural changes and doping are summarized in this section. The materials in the following paragraphs are arranged in size order, from nanoparticles up to hollow microspheres.

The metals that other researchers added to these composites were unlike those used in the research of Li et al. [47]. Their method greatly improved the material's photocatalytic properties. In 2015, they inlaid Pt (Pd) nanoparticles with sizes of approximately 3 nm (5.5 nm) into ZnO nanoparticle–rGO sheet composites to improve their photocatalysis performance. In the synthesis process, $\text{Zn}(\text{Ac})_2 \cdot 2\text{H}_2\text{O}$ was added to a graphite oxide solution made from graphite powder, and the pH was adjusted to 9. After sonication for 30 min, a K_2PtCl_4 (K_2PdCl_4) solution was mixed into the previously prepared solution, and the resulting mixture was processed by a one-pot hydrothermal method under autogenous pressure. The synthesis route for the Pt/ZnO/graphene nanosheet (GN) and Pd/ZnO/GN composites is illustrated in Figure 8a.

When compared with previously described dopant substances, the dopants used by Bhirud et al. [48] were particularly specialized and very effective. In 2015, they synthesized photocatalysts by embedding nitrogen-doped ZnO nanoparticles with sizes ranging from 4 to 9 nm into graphene sheets. In the synthesis process, a 0.5 M ZnCl_2 ethanol solution and urea were mixed, with the weight ratio of ZnCl_2 to urea being 1:2. Then, graphene oxide dispersed in ethanol was added to this mixture. The resulting solution was first stirred for 30 min and then placed into an oven at a temperature of 150 °C. After baking, the product that was removed from the oven was first dried in a desiccator and then annealed at 500 °C for 3 h.

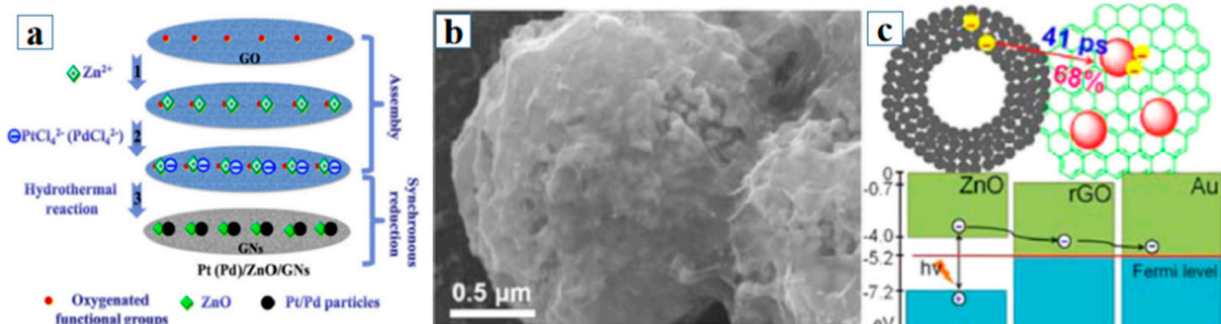


Figure 8. (a) Synthesis route for the Pt/ZnO/graphene nanosheet (GN) and Pd/ZnO/GNs composites; (b) SEM image of structure of ZnO–rGO hollow microspheres with Au nanoparticles; (c) energy band and structural principle of the ZnO–rGO hollow microsphere composite with Au nanoparticles.

ZnO–2D graphene sheets were fabricated using a combination of doping and structural change in 2014 by Khoa et al. [40], who decorated ZnO–rGO hollow microspheres with Au nanoparticles to act as pollutant degradation photocatalysts, where the atomic contents of Au and C were 9% and 13.3%, respectively. An SEM image of the material composed of ZnO–rGO hollow microspheres with Au nanoparticles is shown in Figure 5b. Hollow ZnO microspheres with a size of 1.6 μm were first formed by chemical deposition. Subsequently, a ZnO ethanol solution was combined with a precursor solution produced by mixing an rGO aqueous solution, hydrogen tetrachloroaurate (III), and tetra-n-butylammonium bromide, which can not only combine graphene oxide with ZnO but can also avoid aggregation of the graphene. The energy bands and structural principles of the ZnO–rGO hollow microsphere material with Au nanoparticles are shown in Figure 8c. The structures involving hollow microspheres have proved both promising and highly useful.

3.3. ZnO–3D Graphene Foam

ZnO–graphene composites in which the graphene has a 3D structure offer specific beneficial effects for light absorption when compared with other ZnO–graphene composites. The foam-like structure can not only prevent the agglomeration problem for graphene but can also help the ZnO nanocrystal seeds to penetrate and attach to the graphene [31]. In recent years, researchers have changed the ZnO shape to form heterostructures with graphene, including ZnO nanowire–3D graphene networks, ZnO NR–3D graphene networks, and ZnO quantum dot–3D graphene networks. Each form of the resulting ZnO–3D graphene foams has specific advantages.

3.3.1. ZnO Quantum Dot–3D Graphene Network

Zero-dimensional ZnO QDs and 3D graphene can form a good composite contact. In 2015, Tayyebi et al. [49] used ZnO QDs with a size of 3 nm to decorate graphene films for photocatalysis applications. To synthesize these composites, the graphene oxide, which was initially prepared from graphite powder, was dispersed in 100 mL of anhydrous DMF. The resulting graphene oxide suspension was then subjected to ultrasonication for 15 min. Simultaneously, a zinc acetate solution was prepared by mixing 1 g of zinc acetate with 100 mL of DMF and 20 mL of deionized water. Finally, a mixture of the graphene oxide suspension and this zinc acetate solution was subjected to hydrothermal processing at 95 °C for 5 h.

3.3.2. ZnO Nanowire–3D Graphene Network

The preparation of ZnO nanowires has been studied widely, and the researchers found that the ZnO nanowire–3D graphene network structure had excellent development prospects. In 2015, Boruah et al. [50] fabricated a photodetector by growing ZnO nanowires on a 3D graphene network. First, a nickel foam was cleaned and then coated with graphene using an atmospheric CVD process. The foam was then covered with PC and immersed in a HCl solution to remove the nickel. Etching of the PC was achieved by dipping the foam into chloroform, and a self-supporting graphene foam was thus obtained. Finally, ZnO nanowires with diameters of 10–30 nm and lengths of a few microns were grown on the graphene foam using a vapor-solid evaporation approach. A schematic of the steps involved in fabrication of the ZnO nanowire–3D graphene network samples is shown in Figure 9a.

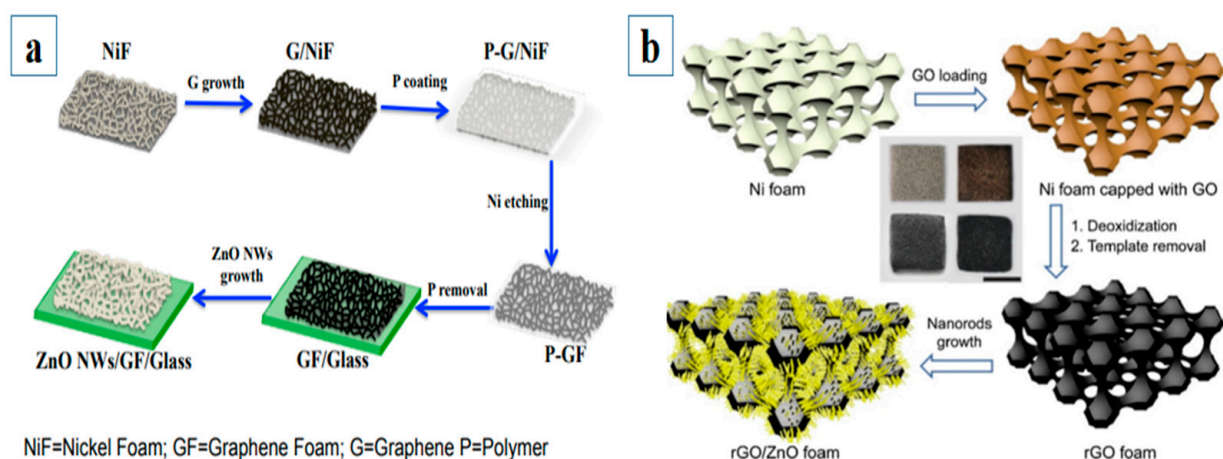


Figure 9. (a) Schematic of steps involved in ZnO nanowire–3D graphene network sample fabrication; (b) schematic diagram of preparation of the free-standing ZnO/rGO foam.

Li et al. [7] fabricated a piezoelectric nanogenerator based on ZnO nanowires grown on a graphene network in 2015. Their method for fabrication of the ZnO nanowire–3D graphene network was entirely different to that of Boruah et al. First, a graphene oxide

sheet was deposited on a polyurethane (PU) sponge with a pore size of 500 μm and a 150 μm fiber diameter by dipping the sponge into a graphene oxide solution and then drying it for 6 h at 80 $^{\circ}\text{C}$. The graphene oxide layer was then reduced via a vitamin-C-based reduction method. ZnO nanowires with diameters of 855 ± 192 nm were subsequently grown on the inner surface of the sponge via hydrothermal synthesis, and the areal density of these ZnO nanowires was approximately $(7.1 \pm 0.8) \times 10^7$ cm^{-2} . The remaining space was backfilled using polydimethylsiloxane (PDMS), which can not only protect the ZnO nanowires from disruption but can also serve as a stress concentrator to enhance the power density per unit area.

The method used by Shao et al. [51] to grow a ZnO nanowire–3D graphene network was similar to that of Boruah et al. However, to improve the catalytic performance of their material, they doped this structure with elemental Cl. In 2015, Shao et al. grew Cl-doped ZnO nanowires on a graphene foam, and the material showed high photocatalysis efficiency. In 2016, Song et al. [31] inlaid ZnO nanowires on a 3D graphene foam, and the electromagnetic wave absorption of the resulting composite was measured and analyzed.

3.3.3. ZnO Nanorod–3D Graphene Network

In 2015, Cai et al. [52] deposited ZnO NRs with an average diameter of 500 nm on a 3D graphene network for photocatalysis applications. First, a nickel foam, which served as the template for 3D graphene network growth, was immersed in isopropanol, acetone, absolute ethyl alcohol, and deionized water and was then ultra-sonicated, heated, and annealed to clean it. A CVD approach was then used to grow graphene on the nickel foam, and ethanol was used as a precursor. To obtain a self-standing 3D graphene network, the nickel foam was etched away using a HCl solution. Finally, ZnO NRs were embedded in the graphene foam through a hydrothermal process using ammonia and ZnCl_2 .

Men et al. [53] grew ZnO NRs with diameters of approximately 100 nm on a 3D graphene foam for photocatalysis applications. The graphene foam was first synthesized by immersing a nickel foam in a graphene oxide solution and then performing a reduction process using hydrazine in 2015. To produce a self-supporting graphene foam, the Ni foam was removed using a mixture of FeCl_3 and HCl. The ZnO NRs were then deposited in the graphene foam via the hydrothermal method. The ZnO seed solution was a mixture of a NaOH ethanol solution and a $(\text{CH}_3\text{COO})_2\text{Zn}$ ethanol solution, while the ZnO nanorod precursor solution was a mixture of $\text{Zn}(\text{NO}_3)_2 \cdot 6\text{H}_2\text{O}$ and hexamethylenetetramine. A schematic diagram of the process for preparation of the free-standing ZnO/rGO foam is shown in Figure 9b.

The existence of the 3D structure in the ZnO–3D graphene foam has specific beneficial effects for light absorption when compared with other ZnO–graphene composites. When compared with other similar structures, there has been little research on doping with metal nanoparticles.

4. Photocatalysis

4.1. ZnO–0D Graphene Quantum Dot Photocatalysts

In the preceding section, the methods for optimization of the ZnO–0D graphene QD materials are divided into structural-change-based and doping-based methods. In the following, the advantages of the ZnO–0D graphene QD structures are described using the structural change and doping aspects. Additionally, the physical property information and performance statistics of these ZnO–graphene materials with their different structures are listed in Table 1.

In terms of the structural change aspect, the ZnO–GQD composites synthesized by Ebrahimi et al. [38] demonstrated photocatalytic efficiency that was three times higher than that of the ZnO nanowires alone. The working mechanism of the ZnO–GQD composites is shown in Figure 10a. The reasons for this enhancement are listed as follows: (a) Because of the quantum confinement effect, the band gap energy of the GQDs changed to approximately 2.2 eV, which allowed the composites to harvest visible light; (b) the ZnO–GQD structure induced electrons in the ZnO conduction band to move to the highest

occupied molecular orbital (HOMO) of the GQDs and combine with the holes generated in the GQDs, meaning that recombination was reduced in both ZnO and the GQDs. In addition, the Zn–O–C bonds formed in this structure reduced oxygen activation on the surface and improved the structural stability. Variation of $\ln(C_0/C)$ vs. reaction time under solar irradiation for the ZnO NWs and GQDs/ZnO NWs with different GQD loadings is shown in Figure 10d. According to the first-order Langmuir–Hinshelwood kinetics ($\ln(C_0/C) = kt$), a higher K value means a greater photocatalytic degradation rate. C is the methylene blue (MB) concentration at any time t, and C_0 is the primary concentration of MB. K is the first-order degradation rate constant.

Table 1. Physical properties information and performance statistics of ZnO–graphene materials with various structures.

Structure	Diameter of ZnO (Synthesis Method)	Graphene Content	Mass/Concentration of Sample	Target Pollutant	Detection Light	Performance	Ref.
Ag nanoparticles–0D graphene–ZnO flowers	\	0.1 mg·mL ⁻¹ GQDs aqueous solution	\	Rhodamine B (RhB)	500 W visible light	Efficiency of 57.49% after 8 h of illumination	[35]
ZnO nanowires–0D graphene	170–250 nm (anodization)	0.4 wt% GQDs	15 mg	40 mL 10 ⁻⁵ M methylene blue (MB) solution	800 W·m ⁻² solar light	First-order degradation rate constant (k) = 0.007 min ⁻¹ (180 min illumination)	[38]
ZnO nanoparticles–2D graphene core-shell	500 nm (one-step wet chemical method)	10 mg graphene oxide	0.1 g	100 mL 10 mg·L ⁻¹ RhB solution	300 W Xe arc lamp	Achieved 78.9% degradation within 10 min and finished after 20 min	[15]
ZnO nanowires–2D graphene	1.8 µm (33.8 µm length) (PVP-assisted water solution thermal method)	\	10 mg	100 mL 10 mg/L Rhodamine 6G (Rh6G) solution	A 150 W mercury lamp with wavelength of 365 nm	Achieved 80% efficiency after 5 min and 98% after 10 min	[54]
Micro-sized ZnO flowers–2D graphene	Simple one-pot hydrothermal method	2% graphene oxide	50 mg	40 mL 15 mg·mL ⁻¹ MB solution	a 100 W UV lamp	Completed in 60 min	[18]
ZnO quantum dots–2D graphene	3 nm (simple chemical method)	5% graphing loading	50 mg	100 mL of a 1.5 × 10 ⁻⁴ M aqueous methyl orange (MO) solution (pH = 6.5)	100 W mercury lamp with the wavelength of 365 nm as the UV source; a 175 W metal halide lamp (λ > 420 nm) as the visible light source	degradation rate = 0.11 min ⁻¹ under UV light; degradation rate = 0.35 h ⁻¹ under visible light	[49]
ZnO nanorods–2D graphene	16 nm (solvothermal method)	10 wt% graphene	60 mg	50 mL 10 mg·L ⁻¹ Orange II solution	5 mW·cm ⁻² solar light	Efficiency of 99% after 150 min illumination	[55]
Hierarchically structured ZnO–2D graphene hollow microspheres	Individual ZnO nanoparticles: 12 nm; microspheres: over 50 nm (low-temperature solution method)	Graphene oxide to zinc acetate dihydrate weight ratio = 0.032	1 mg·mL ⁻¹	10 ⁻⁵ M RhB solution, 10 ⁻⁵ M MO solution, 10 ⁻⁴ M phenols solution	UV light with wavelength of 254 nm	Completed in 40 min; constant first-order rate = 6.2 × 10 ⁻² min ⁻¹ ; 1.5 × 10 ⁻² min ⁻¹	[17]
ZnO nanoparticles–2D graphene	10–20 nm (a simple one-step hydrothermal method)	0.3 wt% graphene	25 mg	50 mL 15 ppm deoxyribovalenol (DON) aqueous solute	UV light with wavelength of 254 nm and 365 nm	Reaction rate constant: 0.10411 min ⁻¹ under 365 nm light; 0.024 min ⁻¹ under 254 nm light	[56]
ZnO nanorods–carbon nanotubes–2D graphene	40–60 nm (microwave-assisted hydrothermal method)	\	1.5 g·L ⁻¹	100 mL 5 mg·L ⁻¹ MB solution	500 W Hg lamp produced UV light with wavelength of 365 nm	96% efficiency for 3.9 wt% carbon nanotubes in 160 min illumination	[41]
ZnO nanoparticles–Au nanorods–2D graphene	45.3 ± 3.7 nm (simple one-pot hydrothermal method)	0.5 mg·mL ⁻¹ graphene	4 mg·mL ⁻¹ in methanol	5 mM 50 mL nitrobenzene (NB) in methanol solution	500 W UV–Vis lamp with the wavelength above 420 nm	Achieved 97.8% efficiency with 18 mM ZnO and 0.5 mM Au	[45]
ZnO nanorods–CdS–2D graphene	95 degree refluxing method	5 wt% graphene	10 mg with 40 mg HCOONH ₄ (hole scavenger)	40 mL 10 mg·L ⁻¹ aromatic nitro compounds solution	300 W Xe arc lamp with wavelength less than 420 nm	95% efficiency (16 min illumination)	[19]

Table 1. Cont.

Structure	Diameter of ZnO (Synthesis Method)	Graphene Content	Mass/Concentration of Sample	Target Pollutant	Detection Light	Performance	Ref.
Ag nanoparticles–ZnO nanorods–2D graphene	Low-temperature microwave-assisted solution method	1 wt% graphene oxide	50 mg	50 mL 20 mg·L ⁻¹ MO solution	300 W 365 nm-wavelength Hg lamp	94.8% efficiency for the first text, 91.7% efficiency for the fifth text (80 min illumination for each test)	[46]
ZnO–2D graphene hollow microspheres with Au nanoparticles	Individual ZnO nanoparticles: 50 nm; microspheres: 1.6 μm	The atomic contents of Au and C were 9% and 13.3%	\	10 mL 10 μM MB solution	20 W black-light (UVA) lamps (wavelength range 315–400 nm)	68% efficiency	[40]
ZnO nanoparticles–Pt (Pd) nanoparticles–2D graphene	One-pot hydrothermal method	50 mg graphene oxide	\	1.0 M methanol solution	0.3 mW·cm ⁻² UV light with wavelength of 250–270 nm and visible light with wavelength over 420 nm	\	[47]
Nitrogen doped ZnO nanoparticles–2D graphene	4–9 nm (facile wet chemical method)	0.3% graphene	0.2 mg	200 mL 0.25 M aqueous KOH bubbled by hydrogen sulfide (H ₂ S) for about 1 h at the rate of 2.5 mL min ⁻¹ at 299 K	300 W visible light	Hydrogen evolution rate of 5072 μmol·h ⁻¹	[48]
ZnO nanorods–3D graphene	100 nm (hydrothermal method)	\	0.2 mg·mL ⁻¹	25 mL 5 ppm RhB solution	100 mW·cm ⁻² simulated solar light	Over 95% efficiency in 150 min illumination	[53]
Cl-doped ZnO nanowires grown on 3D graphene	40–100 nm (hydrothermal method)	\	2 cm × 2 cm	50 mL 5mg·L ⁻¹ RhB solution	A 150 W xenon lamp for UV irradiation	Finished within 75 min	[51]
ZnO nanorods–3D graphene	500 nm (hydrothermal method)	\	6 mg·mL ⁻¹	20 mL 5 mmol·L ⁻¹ MO solution	300 W UV light with wavelength of 365 nm	92% efficiency in 180 min illumination	[52]

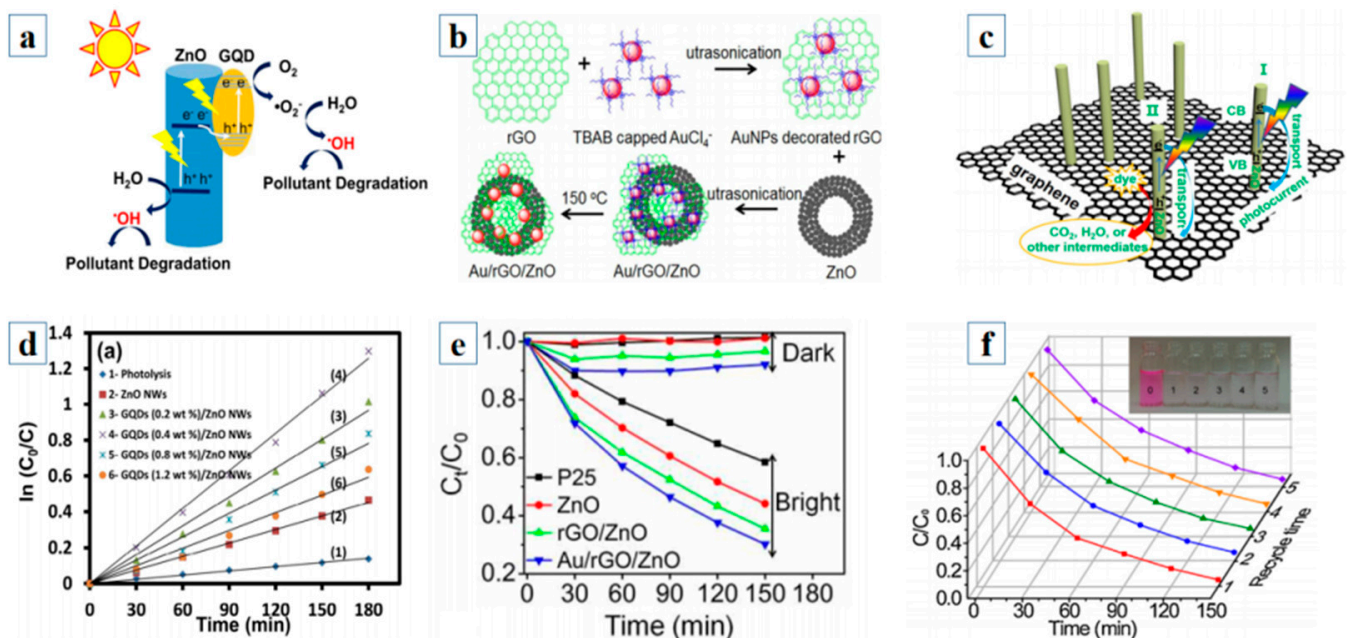


Figure 10. (a) The working mechanism of the ZnO–GQD composites; (b) schematic illustration of the synthesis of Au/rGO/ZnO hybrid; (c) schematic illustration of the photocatalytic mechanism of the ZnO/rGO foam; (d) variation of $\ln(C_0/C)$ vs. reaction time under solar irradiation for the ZnO NWs and GQDs/ZnO NWs with different GQD loadings; (e) photocatalytic performance of ZnO samples (ZnO, rGO/ZnO and Au/rGO/ZnO) compared with P25; (f) recyclable photodegradation of the ZnO/rGO foam for the first, second, third, fourth, and fifth cycles.

Wang et al. [35] prepared ZnO–GQDs by changing the original structure and doping it with Ag metal. Use of the plasmon resonance effect of the metal nanoparticles allows the optical properties of the materials to be greatly enhanced. In 2015, Wang et al. synthesized Ag nanoparticle–GQD–ZnO flower ternary composites for photocatalysis applications in visible light. The presence of Ag not only inhibits the aggregation of ZnO but also helps the composite to harvest visible light. In addition, because of energy level differences, the holes that are generated in the ZnO travel to the Ag, while the electrons that are generated in the Ag travel to the ZnO and the GQDs, meaning that recombination is reduced. The GQDs with their electronegativity induce the Ag ions and ZnO cores to be distributed evenly and thus reduce the sizes of the Ag nanoparticles and ZnO flowers that are ultimately formed. Furthermore, the electronegativity of the GQDs reduces the polarity of the solution, and the composites thus present isotropic characteristics.

4.2. ZnO–2D Graphene Sheet Photocatalysts

This type of photocatalyst is composed of composites with different ZnO structures embedded on or covered by 2D graphene sheets, including sandwich-like ZnO nanoparticle–graphene–ZnO nanoparticles [42] and ZnO nanoparticle–graphene core-shell [15], ZnO nanowire–graphene [54], micro-sized ZnO flower–graphene [18], ZnO QD–graphene film [49], ZnO NR–graphene [55], hierarchically structured ZnO–graphene hollow microsphere [17], and ZnO nanoparticle–graphene sheet [56] hybrids. The photocatalytic mechanisms of these materials for high degradation efficiency are similar. First, because of their large direct band gap, it is easier for the ZnO nanocrystals to absorb photons with high energy. Second, both the ZnO nanocrystals and the graphene sheets have high surface-to-volume ratios, which contribute to their high efficiency. Third, the high recombination problem of ZnO related to its direct bandgap can be alleviated by combining it with graphene, which has high carrier mobility. Furthermore, the recombination problem can be mitigated by the energy level difference and the electric field that forms at the composite between graphene and ZnO [15]. Ultimately, combining ZnO with graphene protects both materials from aggregation [31]. Among these structures, the sandwich-like ZnO–2D graphene–ZnO nanocomposites synthesized by Wu et al. [42] should be highlighted because they can protect the graphene from air oxidation. Additionally, Bu et al. [15] and Xu et al. [18] operated based on a similar foundation that addition of the graphene oxide during the synthesis process would be appropriate. On the one hand, addition of too little graphene oxide causes the ZnO nanoparticles to combine more closely and then form larger composites that influence the efficiency because the negative charge sites induced by the graphene oxide would combine with the zinc ions and thus reduce their concentration. On the other hand, addition of too much oxide causes the graphene layer to be too thick and generate a surplus section between the ZnO aggregates that would hinder pollutants from reaching the ZnO.

Other substances including metals, compounds, and carbon nanotubes can be added to the ZnO–2D graphene composites to achieve lower recombination rates [40,41,45–47], higher light absorption [40,41], visible light absorption [19,47,57], and reduced photocorrosion of ZnO [19]. Therefore, the performances of the ZnO–2D graphene composites can be explained in terms of three aspects: the addition of the metals, compounds, and carbon nanotubes.

4.2.1. ZnO–2D Graphene Doped with Metals

Various metals are used as dopant materials, including Au and Ag. Additionally, in certain specific circumstances, the metals can form a surface plasmon resonance effect with the rest of the materials. Roy et al. [45] synthesized ZnO nanoparticle–graphene sheet–Au NR composites. Because the Au work function is lower than that of graphene, a contact composed of the Au NRs and a graphene sheet causes further separation of the electrons and holes excited in ZnO and therefore enhances the photocatalytic efficiency. The Au–ZnO–graphene hybrid material synthesized in their work exhibited efficiency

that was 3.5 and 4.5 times higher than that of commercial TiO₂ and ZnO nanospheres, respectively. Khoa et al. [40] synthesized hierarchically structured ZnO–graphene–Au hollow microspheres and the composites formed showed better performance than P25. A schematic illustration of the synthesis of Au/rGO/ZnO hybrid is shown in Figure 10b. In addition to the remarkable conductivity of Au, a reason for the remarkable photocatalytic performance of the composite is that photons impinging on the Au nanoparticles are trapped or scattered at the interface because of the plasmonic light trapping effect and thus improve the absorption of light. Furthermore, the surface defects in ZnO can help the electrons in the ZnO conduction band to transfer to the Au/rGO layer. Photocatalytic performance of ZnO samples (ZnO, rGO/ZnO, and Au/rGO/ZnO) compared with P25 is shown in Figure 10e.

4.2.2. ZnO–2D Graphene Doped with Compounds

Materials doped with different compounds offer a variety of different advantages. In 2014, to improve the photocatalytic performance of ZnO-based devices in the visible light region, Han et al. [19] decorated ZnO nanorods that were embedded in a 2D rGO sheet with CdS, i.e., a material with a smaller bandgap. CdS can help to absorb the visible light, while graphene plays the role of recombination inhibitor. In addition, because the valence band of CdS is higher than that of ZnO, the holes that are created in ZnO shift to CdS and thus prohibit photocorrosion in ZnO. Li et al. [47] synthesized Pt nanoparticle (Pd nanoparticle)–ZnO nanoparticle–rGO sheet composites. When the samples were illuminated, they presented reduced current density decay, thus indicating catalyst stability. The CO oxidation potential of the Pt (Pd)–ZnO–graphene composite shows its tolerance to the CO-like species. The electrons that were transferred from the ZnO conduction band to the Pt nanoparticles (Pd nanoparticles) could not only inhibit ZnO recombination but also could reduce partially oxidized Pt (Pd) and maintain its electrocatalytic activity. Additionally, the ZnO bandgap is narrowed after contact with graphene and Pt (Pd) and exhibits absorption of visible light, particularly UV radiation.

After researchers had doped their composites with CdS and Pt nanoparticles (Pd nanoparticles), in 2015, Bhirud et al. [48] caused their ZnO–rGO sheet nanocomposites to absorb visible light by doping the ZnO nanoparticles with nitrogen. Because of the use of doping, a new energy level, N 2p, was generated between the valence and conduction bands of ZnO. Therefore, the electrons in the ZnO valence band can first be excited to the N 2p level and then be excited further by the visible light photons to the ZnO conduction band.

4.2.3. ZnO–2D Graphene Doped with Carbon Nanotubes

In 2012, Lv et al. [41] synthesized ZnO NR–carbon nanotube–2D graphene composites to improve the photodegradation efficiency of methylene blue. The participation of the carbon nanotubes not only leads to higher light absorption but also offsets the weak electron mobility of rGO that occurs because of incomplete reduction. Additionally, similar to the role of the Au NRs in the work by Roy et al. [45], the carbon nanotubes cause the electrons generated in ZnO to be separated further because the carbon nanotubes have an even lower work function than that of rGO. Based on these advantages, the ZnO–rGO–carbon nanotube composites offer higher efficiency for methylene blue photocatalytic decomposition than the pure ZnO–rGO structure.

4.3. ZnO–3D Graphene Photocatalysts

The advantages of the ZnO–3D graphene structure for use in photocatalysis are described based on the structural change and doping aspects. To improve the properties of their material by changing its structure, Men et al. [53] synthesized a ZnO nanorod–3D graphene hybrid, which was self-supporting and did not need an extra substrate, and the photocatalysis performance of this hybrid was tested. A schematic illustration of the photocatalytic mechanism of the ZnO/rGO foam is shown in Figure 10c. This structure not only retains the advantages of the ZnO–graphene sheet composites but also helps

both the reaction solution and the light to penetrate the composite deeply through its porous network. In addition, the porous network causes reflected light to scatter inside it to increase light utilization. Because of these beneficial characteristics of 3D graphene, the ZnO–graphene foam produced a higher photocurrent than the ZnO–graphene sheet under the same conditions. The composites also showed excellent performances in degrading RhB and in recycling experiments, which demonstrated their stability and reusability. Recyclable photodegradation of the ZnO/rGO foam for the first, second, third, fourth, and fifth cycles is shown in Figure 10f. However, the optical properties of these materials can also be enhanced by doping.

After many researchers prepared ZnO–3D graphene structures, Shao et al. [51] optimized their structure using a combination of structural change and doping and then explored the photocatalysis of the material. In 2015, Shao et al. [51] synthesized Cl-doped ZnO nanowire–graphene foam composites that showed higher photocatalysis efficiency than the pure ZnO nanowire–graphene foam composites. In addition, these composites do not need to be removed from the reaction solution after use and also maintain excellent recyclability. In this mechanism, first, the graphene network and the surface defects in the ZnO nanowires can attract and trap electrons and holes, respectively. Therefore, the recombination rate can be reduced, and high photocatalysis efficiency can thus be realized. Second, the Cl doping can not only increase the number of electrons in the ZnO conduction band but can also ease the electron transport process in the ZnO nanowires. Furthermore, Cl doping led to an increased density of grown and surface defects in the ZnO nanowires.

As mentioned above, the photocatalytic ability of semiconductors is highly dependent on the formation and transportation processes of photogenerated carriers. ZnO–graphene just happens to meet these requirements. By tuning dimension, graphene exhibits semiconductor characteristics. On the one hand, ZnO–graphene composites can exhibit type II band alignment, and the separation and transportation of electrons and holes may be distinguished. In this band structure, electrons in the ZnO conduction band can move to the highest occupied molecular orbital (HOMO) of the graphene (GQDs) and combine with the holes generated in the GQDs, meaning that recombination was reduced in ZnO and GQDs. On the other hand, ZnO–graphene composites are also allowed to harvest visible light, which achieves the purpose of extending the absorption spectrum range. Third, morphologically diverse graphene can be applied with higher surface-to-volume ratio and increase the adsorption capacity. Furthermore, doping with compounds is an effective method to enhance the performance of photocatalysis. For example, doping N and Cl not only increases the number of electrons in the ZnO conduction band but can also ease the electron transport process in the ZnO via doping N and Cl to generate a new energy level. In addition to doping compounds to enhance the performance of photocatalysis, structural change can increase the interfacial contact area of ZnO and graphene, which causes further separation of the electrons and holes excited in ZnO.

5. Photodetection

5.1. ZnO–0D Graphene Quantum Dot Photodetector

The ZnO–0D graphene QD structures have close interface contact that is conducive to carrier transport. Therefore, devices based on ZnO–0D graphene QDs can have excellent photoelectric properties. Dhar et al. [37] synthesized a UV detector based on a QD–ZnO nanorod composite that exhibited better performance than photodetectors based on pure ZnO nanorods in 2016. The participation of the GQDs not only increases the number of electron–hole pairs that are generated because of the quantum confinement effect but also creates an energy level gap that moves the electrons to ZnO and the holes to the GQDs. Additionally, under reverse bias, the Schottky junction between the GQDs and the ZnO nanorods can cause the depletion region to shrink to such a degree that electron tunneling occurs.

After Dhar et al. completed their research, Ghosh [39] decorated ZnO nanorods with GQDs to produce a photodetector with remarkably high performance. GQDs (G1) were

synthesized by high pressure microwave irradiation of citric acid as the building block and ethanolamine as the capping agent. First, this enhanced performance is due to the electron–hole pairs generated in the QDs under UV irradiation via the quantum confinement effect. Second, because the lowest unoccupied molecular orbital (LUMO) and HOMO of the QD are higher than the conduction and valence bands of ZnO, respectively, the electrons in the QDs are transferred to ZnO to enhance the photoresponse, while the holes in ZnO are transferred to the QDs to release the absorbed oxygen molecules and thus reduce recombination. Third, when compared with graphene sheets, QDs have intimate contact with ZnO, which aids charge transference. The current density versus potential curves are shown in Figure 11a. Additionally, the relationships between responsivity and wavelength for both ZnO and ZnO–G1 are shown in Figure 11b. It is obvious that the responsivity of the ZnO–G1 composite is five times higher than that of ZnO alone.

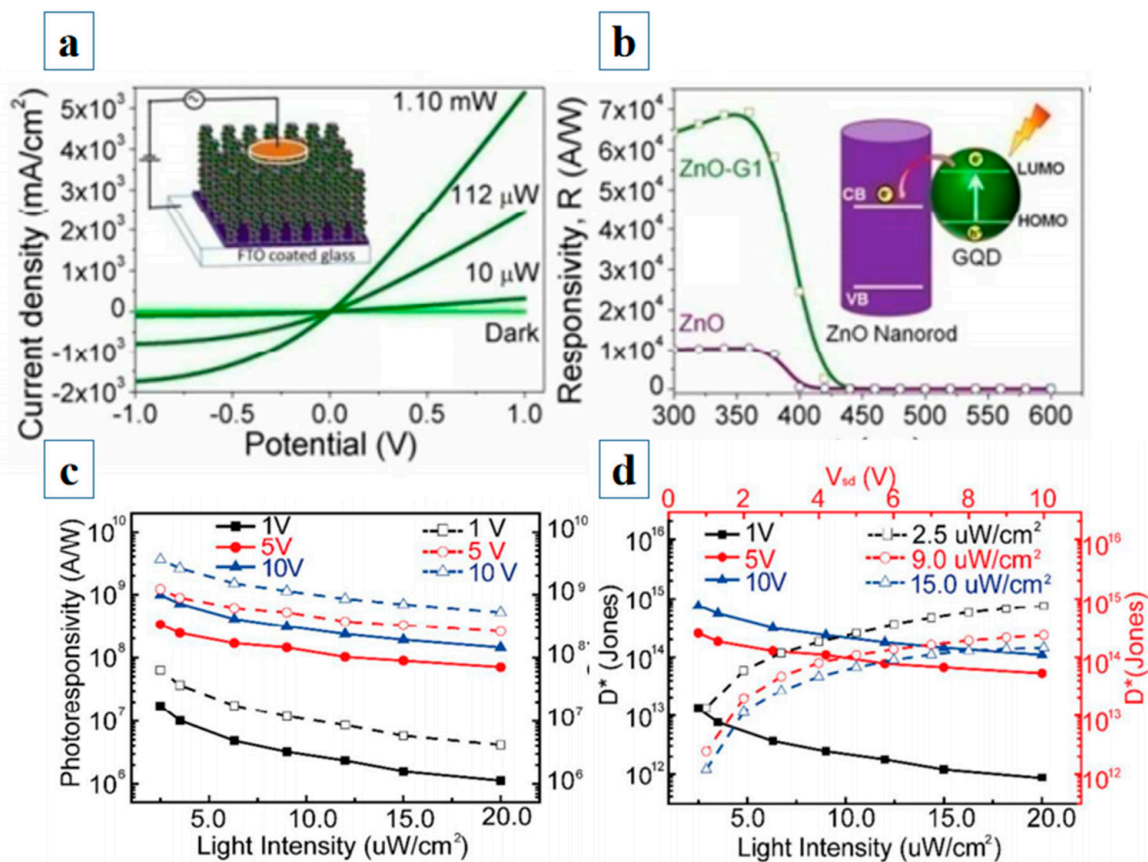


Figure 11. (a) ZnO–G1 under illumination by 365 nm UV light at different intensities. The inset shows a schematic of the device; (b) relationship between responsivity and wavelength for ZnO and ZnO–G1. The inset shows a schematic of electron transfer from a GQD to the ZnO nanorods; (c) photoreponsivity (solid with left-hand scale) and gain (dashed with right-hand scale) as functions of the UV light intensity at different V_{sd} ; (d) detectivity D^* as a function of the UV (340 nm) light intensity (black axis and solid curves) and V_{sd} (red axis and dashed curves).

Gong et al. [58] fabricated a photodetector with a ZnO QD–graphene sheet structure, and their device presented an excellent photosensing performance that was attributed to the quantum confinement effect of the ZnO QDs, which brought enhanced light absorption, tunable spectra, and increased charge mobility. Furthermore, enhancement of the photodetection performance was accomplished by successfully removing the zinc acetate dihydrate ($Zn(Ac)_2$) layer sandwiched between the ZnO QDs and the graphene sheet. This layer medium is composed of the residue from solution synthesis and obstructs electrons traveling from the ZnO conduction band to the graphene sheet. Through formation of a clean van der Waals interface, exciton dissociation and electron transfer can both be

ensured. The photoresponsivity (solid with left-hand scale) and the gain (dashed with the right-hand scale) are shown in Figure 11c as functions of the UV light intensity at different V_{sd} . Additionally, the detectivity D^* is shown as a function of the UV (340 nm) light intensity (black axis and solid curves) and V_{sd} (red axis and dashed curves) in Figure 11d.

5.2. ZnO–2D Graphene Photodetectors

The devices in this section vary in both structure and synthesis processes, resulting in various advantages in terms of the different properties of the resulting photodetectors. In the following sections, ZnO nanowire–graphene sheet photodetectors and ZnO nanorod–graphene sheet photodetectors are described.

5.2.1. ZnO Nanowire–Graphene Sheet Photodetectors

Xu et al. [43] fabricated a photodetector based on ZnO nanowire–graphene sheet hybrid structures that were sandwiched between the two 200 nm-thick Au electrodes of a Schottky contact. This device presented a better dark current performance, photocurrent-to-dark current ratio, and UV-to-visible rejection ratio than photodetectors made using ZnO nanowires grown on p-type silicon substrates with SiO_2 layers. In addition to the high mobility of graphene, a reason for this performance improvement is that the ZnO nanowires have better crystal quality if they are grown on a graphene sheet rather than on a silicon substrate with a SiO_2 layer. Further credit should be attributed to the surface plasma that occurs at the interface between the graphene layer and ZnO, which can create an electromagnetic field in the ZnO nanowires and thus increase light absorption.

Boruah et al. [44] further improved the electrical properties and stability of their device by changing the ZnO nanowire–graphene structure. They fabricated a self-powered high-sensitivity UV photodetector with a graphene sheet–ZnO nanowire–graphene sheet sandwich structure. This sandwich structure not only avoids the problem of the high dark current due to the existence of a metal electrode–graphene–metal electrode route but also eliminates the slow response problem due to the high substrate resistivity. In addition, the near-zero response current change in the cyclic experiment demonstrates the detector's excellent stability and reproducibility. The research also found that the detector's recovery time is initially fast but gradually slows, thus indicating that with the exception of direct band-to-band recombination, there is an indirect oxygen participant mechanism that can eliminate the electrons and holes slowly. (An oxygen molecule in air reacts with an excited electron to form O^{2-} and is then oxidized by a hole on the ZnO nanowire surface) Finally, the research also found that light intensities that are too low or too high are not beneficial to the photoresponse because they lead to insufficient numbers of excitons and improved charge recombination due to self-heating-induced carrier scattering, respectively.

Cook et al. [59] also improved the ZnO nanowire–graphene structure. They fabricated a ZnO nanowire–ZnO seeded graphene sheet photodetector that presented much better performance than the ZnO nanowire–graphene sheet photodetector without the ZnO seeds. The first reason for this improvement is that the n-doped ZnO seeds increase the number of electrons in graphene and therefore enhance its conductance. The second reason is that because of the presence of the ZnO seeds, the ZnO nanowires that are formed have smaller dimensions and higher density.

5.2.2. ZnO Nanorod–Graphene Sheet Photodetectors

Researchers have grown ZnO on graphene layers using a hydrothermal approach on most occasions. In 2016, to eliminate the problem of the weak interface contact between ZnO and graphene produced by this hydrothermal approach, Yang et al. [2] grew ZnO NRs on an rGO layer (thickness: 2.5 nm; size: $10 \mu\text{m} \times 15 \mu\text{m}$) using a CVD vapor-solid method. A structural schematic of the ZnO NRs/rGO photodetector is shown in Figure 12a. The results obtained for samples grown at different temperatures show that a decline in the growth temperature leads to a reduction in diameter and an increase in density for the ZnO NRs. The small diameter and high density of the ZnO NRs can not only improve

efficiency but can also reduce the leakage current between the substrate and the electrode. A Schottky contact is finally formed, and the oxygen function groups in rGO enhance the p-type properties of the rGO layer and cause the photodetector to be self-powered and to have fast photoresponsivity. Current–voltage (I – V) curves and a time-dependent photocurrent curve of the ZnO/rGO photodetectors are shown in Figure 12b,c.

Liu et al. [60] acknowledged the fast photoresponsivity of the ZnO nanorod–graphene sheet structure. They therefore fabricated a photodetector based on the graphene sheet–ZnO nanorod structure. The effect of strain on the photoresponse of this structure was investigated by calculating the responsivities under conditions with strains ranging from -0.065% to -0.349% under UV illumination with intensity of $25.12 \mu\text{W}\cdot\text{cm}^{-2}$ at a wavelength of 325 nm. They found that the responsivity increased from 71.61 to 84.94 $\text{A}\cdot\text{W}^{-1}$ when the strain decreased from -0.065% to -0.349% with no obvious changes in the rise and fall times. The positive influence of the piezotronic effect on the photoresponse was explained using the higher Schottky barrier height and the broader depletion region at the interface between graphene and ZnO, which enabled separation and transport of the photocarriers.

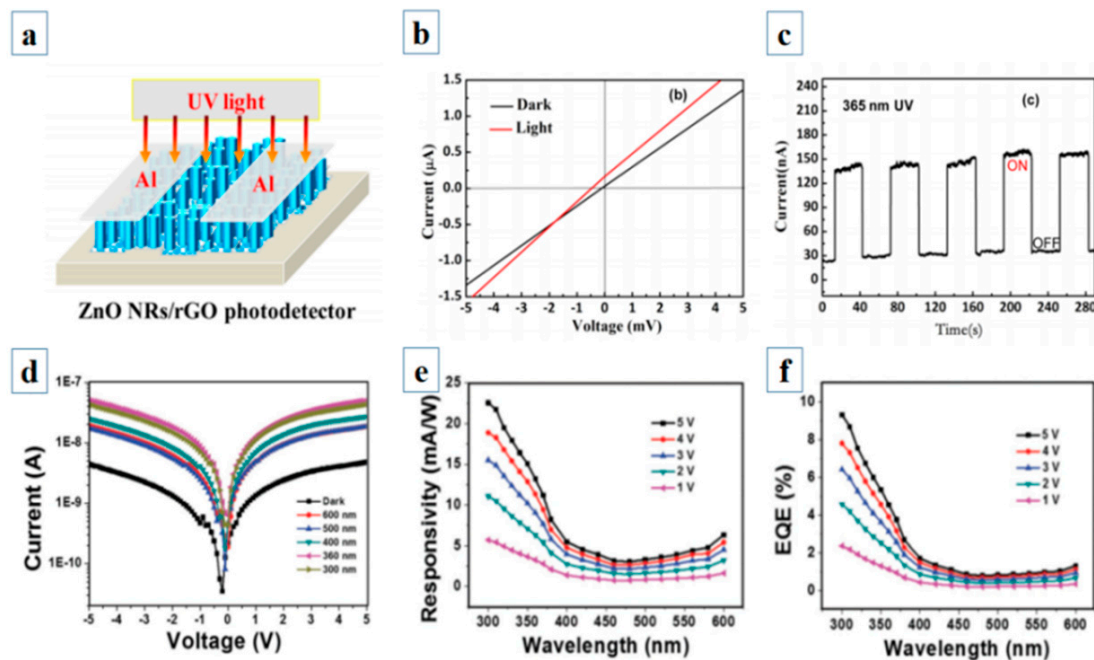


Figure 12. (a) Structural schematic of ZnO NRs/rGO photodetector; (b) I – V curves of ZnO/rGO photodetectors both in the dark and 365 nm UV illumination by sweeping the bias voltage from -5 to 5 mV at a 1 mV scanning rate; (c) time-dependent photocurrent curve of the ZnO/rGO nanohybrid photodetectors at 0 V bias; (d) I – V curves of the ZnO/graphene nanodot array (GNDA; 20 nm) photodetector (PD) in the dark and under light illumination at various wavelengths; (e) responsivity spectra of ZnO/GNDA (20 nm) PD under various bias voltages; (f) EQE spectra of ZnO/GNDA (20 nm) PD under various bias voltages.

5.2.3. ZnO Nanoparticle–Graphene Sheet Photodetectors

Tang et al. [61] fabricated a photodetector based on ZnO nanoparticle–graphene nanodot hybrids. The photosensing performance of the photodetector is related to the size of the graphene nanodots, which can be controlled by varying the etching time. A smaller nanodot size corresponds to a larger energy gap. The graphene nanodots with sizes of 20 and 30 nm had staggered gaps, while the graphene nanodots with a size of 45 nm had a straddling gap. Therefore, the photogenerated holes in the ZnO valence band move to the HOMO levels of the graphene nanodots. Recombination in hybrid materials containing graphene nanodots with sizes of 20 and 30 nm can be prevented because the photogenerated electrons cannot move to the graphene nanodots since their LUMO levels

are higher than the ZnO conduction band. However, because the LUMO level of the 45 nm graphene nanodots is lower than the ZnO conduction band, its recombination rate remains high. Characterization of the photoelectric properties of the ZnO–graphene nanodot array (GNDA; 20 nm) photodetector (PD), including the I – V curves; responsivity; and EQE are shown in Figure 12d–f, respectively.

5.3. ZnO–3D Graphene Photodetector

Boruah et al. [50] fabricated a PD by growing ZnO nanowires on a 3D graphene network. However, under UV light illumination, the high density of the ZnO induced the carriers to travel along the ZnO nanowire–graphene–ZnO nanowire route, which impaired the response time. Under dark conditions, oxygen ion depletion layers formed on the surfaces of the ZnO nanowires because the free electrons absorbed the oxygen molecules and reduced them. Under UV illumination, this oxygen ion depletion layer is reduced because of the oxidation function of the large number of excited holes, while the excited electrons are transferred away to the 3D graphene network. Because the process of absorption of O_2 molecules to eliminate the electrons is much slower than the desorption process, the recovery time is longer than the response time.

In summary, the enhanced performances of ZnO–GQD photodetector are due to the electron–hole pairs generated in the GQDs via the quantum confinement effect and energy band structure of the composite. The LUMO and HOMO of the GQD are higher than the conduction and valence bands of ZnO, which can lead the electrons in the GQDs to be transferred to ZnO to enhance the photoresponse. However, with the increasing size of GQD, the enhancement of photoresponse has a limit on the size of graphene nanodots because the LUMO level of the 45 nm graphene nanodots is lower than the ZnO conduction band, which can lead to high recombination rate. As for other ZnO–graphene photodetectors, increasing the contact area between ZnO and graphene can more effectively improve the performance of photoresponse. Synthesis methods and photoelectric properties statistics of ZnO–graphene materials with different structures is shown in Table 2 clearly.

Table 2. Synthesis methods and photoelectric properties statistics of ZnO–graphene materials with different structures.

Structure	Synthesis Method	Detection Light	Bias	Dark Current or Conductance	Photo Current or Conductance	Photocurrent and Dark Current Ratio	Response Time	Recovery Time	Photo-voltaic Responsivity	Photoconductive Gain	External Quantum Efficiency (EQE)	Ref
ZnO nanorods with QDs	Hydrothermal method	80 mW·cm ⁻² white light	−1 V	0.89 mA·cm ⁻²	13.42 mA·cm ⁻²	15	\	\	36 A/W under illumination with 340 nm wavelength	\	13.161% under illumination with 340 nm wavelength	[37]
ZnO nanorods–QDs	Methanol-assisted hydrothermal method (ZnO), high pressure microwave irradiation of citric acid and ethanolamine (QDs)	365 nm, 10 uW UV light	1 V	2.24 mA·cm ⁻²	320.3 mA·cm ⁻²	142.99	2.14 s at 2 V bias	2.14 s at 2 V bias	6.62 × 10 ⁴ A/W under 2 V bias	\	\	[39]
ZnO nanowires on graphene sheet	Hydrothermal method	370 nm, 0.215 uW UV light	1 V	1.53 nA	3.4 × 10 ⁻⁵ A	2.2 × 10 ⁴	\	\	\	\	\	[43]
ZnO nanowires on graphene sheet	Hydrothermal method + electrophoretic deposition	Solid state lasers with wavelengths of 532, 808, and 1064 nm	\	Saturated current calculated = 2.25 × 10 ⁻⁴ A	\	\	0.1 s for 138 mW laser with wavelength of 532 nm	0.1 s for 138 mW laser with wavelength of 532 nm	0.55, 0.33 and 0.20 mV/W for the 1064, 532, and 808 nm lasers	\	\	[62]
ZnO nanowires on graphene sheet	Resistive thermal evaporation	365 nm, 1.3 mW·cm ⁻² UV light	−5 V	\	\	\	3 s	0.47s	23 A·W ⁻¹ .	\	7845.54%	[44]
ZnO nanorods on graphene sheet	CVD vapor-solid method	365 nm, 10 mW·cm ⁻² UV light	0 V	0.3 uA	0.15 uA	5	0.1 s	0.2 s	\	\	\	[2]
ZnO nanorods on graphene sheet	Magnetron sputtering (ZnO), chemical vapor deposition (graphene sheet), PMMA-assisted method (transference of graphene sheet)	325 nm, 2.93–21.26 uW·cm ⁻² UV light	−1V	4 × 10 ⁻⁶ A with bias of −2 V	\	\	0.3 s	0.5 s	\	\	\	[60]
ZnO quantum dots on graphene sheet	Printing method	340 nm, 15 uW·cm ⁻² UV light	10 V	\	\	1.7	5 s	85.1	9.9 × 10 ⁸ A/W	3.6 × 10 ⁹	\	[58]
ZnO nanoparticles–graphene nanodots	PS NSa-assisted spin-coating method	300 nm	5 V	4.7904 × 10 ⁻⁹ A	4.33 × 10 ⁻⁸ A	9.04	2.5 s under 1 V bias and UV light with wavelength of 360 nm	11 s under 1 V bias and UV light with wavelength of 360 nm	22.55 mA/W	\	9.32%	[61]
ZnO nanowires on ZnO seeded graphene sheet	Floating hydrothermal method	340 nm, 9.89 ± 1.56 uW UV light	5 V	\	6.512 mA	\	\	\	728 A·W ⁻¹	2655	\	[59]
ZnO nanowires on 3D graphene foam	Vapor-solid evaporation	365 nm, 1.3 mW·cm ⁻² UV light	5 V	50.5 uS with zero bias	80.5 uS with zero bias	\	9.5 s	38s	\	\	2490.8% under 8 V bias	[50]

6. Conclusions and Prospects

Photocatalysts and photodetectors based on ZnO–graphene structures exhibit higher efficiency than materials based on either ZnO or graphene alone. Among the ZnO–graphene structures studied to date, ZnO–2D graphene composites have been investigated most thoroughly. With the advantages described in the Introduction, ZnO–2D graphene composites can be improved further by fabricating ZnO in the form of QDs to enhance light absorption and by decorating ZnO with other substances for enhanced visible light absorption and reduced ZnO photocorrosion.

ZnO–0D GQD composites increase light absorption by forming GQD photon harvesters rather than electron transfer structures alone. In addition, the recombination rate is further reduced because of the band structures formed by ZnO and the GQDs. Three-dimensional graphene foam has also been applied as a substrate for ZnO growth in recent years for application to photocatalysts, photodetectors, and nanogenerators. The advantages of the 3D graphene foam are summarized as follows: (a) It is self-supporting and does not require an additional substrate; (b) the agglomeration of the graphene and the density of the composites can both be reduced, leading to large surface areas for the foam; (c) ZnO nanocrystal seeds can penetrate through the foam, which means that the ZnO aggregation problem can be prevented; (d) the porous structure helps both the reaction solution and light to penetrate the composites deeply; and (e) reflected light can be trapped and scattered inside the porous network. Because of these advantages and the fact that there are few studies available to date on ZnO–3D graphene foam nanocomposites, the ZnO–3D graphene structure is promising for use in photocatalysis and photodetection applications.

In brief, significant progress has been made in photocatalysis and photodetection fields for ZnO and ZnO–graphene structures in recent years. However, the band gap of ZnO is still too large and not suitable for absorbing the whole solar band spectra. Therefore, for ZnO–graphene structures, it is necessary to tune band and electronic structures of ZnO. Since black oxide has been developed, an efficient strategy to narrow the band gap of semiconductors has been well recognized. When the surface lattices are disordered, the edges of the conduction and valence band are extended to a forbidden band. In addition, we can tune each band edge through disordered metal and oxygen atoms, respectively. Thus, this disordered ZnO (particles and other nanostructures) should be used to conduct heterojunctions with graphene, which will have greater potential in photocatalysis and photodetection. Several issues must be considered and discussed, for example, the band offset between disordered ZnO and graphene, especially for GODs, the influence of interface of disordered ZnO and graphene on transport of carriers, and how to realize large areas of disordered ZnO–graphene structures.

Author Contributions: Conceptualization, X.F. and D.F.; validation, H.Z. and D.W.; formal analysis, B.L.; investigation, K.Z. and Y.Z.; resources, X.F.; writing-original draft preparation, C.G.; writing-review and editing, C.G. and X.F.; visualization, X.C.; supervision, J.L. and X.W. All authors have read and agreed to the published version of the manuscript.

Funding: This work was funded by the National Natural Science Foundation of China, grant numbers 62074018 and 61274015; the China Postdoctoral Science Foundation funded project, grant numbers 2019M652176 and 2019M661680; the Developing Project of Science and Technology of Jilin Province, grant numbers 20200301052RQ, 20200201266JC, 20190701029GH, 20180519017JH, and 20180520177JH; the Project of Education Department of Jilin Province, grant number JJKH20210831KJ; the Natural Science Foundation of Guangdong Province, grant number 2020A1515010868; and the Shenzhen Fundamental Research Fund, grant number JCYJ20180307151538972.

Conflicts of Interest: The authors declare no conflict of interest.

References

1. Liu, X.; Gu, L.; Zhang, Q.; Wu, J.; Long, Y.; Fan, Z. All-printable band-edge modulated ZnO nanowire photodetectors with ultra-high detectivity. *Nat. Commun.* **2014**, *5*, 4007. [[CrossRef](#)] [[PubMed](#)]
2. Yang, H.; Li, J.; Yu, D.; Li, L. Seed/Catalyst Free Growth and Self-Powered Photoresponse of Vertically Aligned ZnO Nanorods on Reduced Graphene Oxide Nanosheets. *Cryst. Growth Des.* **2016**, *16*, 4831–4838. [[CrossRef](#)]
3. Hmar, J.J.L.; Majumder, T.; Dhar, S.; Mondal, S.P. Sulfur and Nitrogen co-doped graphene quantum dot decorated ZnO nanorod/polymer hybrid flexible device for photosensing applications. *Thin Solid Films* **2016**, *612*, 274–283. [[CrossRef](#)]
4. Qian, L.; Zheng, Y.; Xue, J.; Holloway, P.H. Stable and efficient quantum-dot light-emitting diodes based on solution-processed multilayer structures. *Nat. Photonics* **2011**, *5*, 543–548. [[CrossRef](#)]
5. Lim, J.H.; Kang, C.K.; Kim, K.K.; Park, I.K.; Hwang, D.K.; Park, S.J. UV Electroluminescence Emission from ZnO Light-Emitting Diodes Grown by High-Temperature Radiofrequency Sputtering. *Adv. Mater.* **2006**, *18*, 2720–2724. [[CrossRef](#)]
6. Son, D.I.; Kwon, B.W.; Park, D.H.; Seo, W.-S.; Yi, Y.; Angadi, B.; Lee, C.-L.; Choi, W.K. Emissive ZnO-graphene quantum dots for white-light-emitting diodes. *Nat. Nanotechnol.* **2012**, *7*, 465–471. [[CrossRef](#)]
7. Li, X.; Chen, Y.; Kumar, A.; Mahmoud, A.; Nychka, J.A.; Chung, H.-J. Sponge-Templated Macroporous Graphene Network for Piezoelectric ZnO Nanogenerator. *ACS Appl. Mater. Interfaces* **2015**, *7*, 20753–20760. [[CrossRef](#)]
8. Yang, Y.; Pradel, K.C.; Jing, Q.; Wu, J.M.; Zhang, F.; Zhou, Y.; Zhang, Y.; Wang, Z.L. Thermoelectric Nanogenerators Based on Single Sb-Doped ZnO Micro/Nanobelts. *ACS Nano* **2012**, *6*, 6984–6989. [[CrossRef](#)]
9. Yin, Z.; Wu, S.; Zhou, X.; Huang, X.; Zhang, Q.; Boey, F.; Zhang, H. Electrochemical Deposition of ZnO Nanorods on Transparent Reduced Graphene Oxide Electrodes for Hybrid Solar Cells. *Small* **2010**, *6*, 307–312. [[CrossRef](#)]
10. Wibowo, A.; Marsudi, M.A.; Amal, M.I.; Ananda, M.B.; Stephanie, R.; Ardy, H.; Diguna, L.J. ZnO nanostructured materials for emerging solar cell applications. *RSC Adv.* **2020**, *10*, 42838–42859. [[CrossRef](#)]
11. Guo, J.; Zhang, J.; Zhu, M.; Ju, D.; Xu, H.; Cao, B. High-performance gas sensor based on ZnO nanowires functionalized by Au nanoparticles. *Sens. Actuators B Chem.* **2014**, *199*, 339–345. [[CrossRef](#)]
12. Xia, Y.; Wang, J.; Xu, J.-L.; Li, X.; Xie, D.; Xiang, L.; Komarneni, S. Confined Formation of Ultrathin ZnO Nanorods/Reduced Graphene Oxide Mesoporous Nanocomposites for High-Performance Room-Temperature NO₂ Sensors. *ACS Appl. Mater. Interfaces* **2016**, *8*, 35454–35463. [[CrossRef](#)]
13. Yue, H.Y.; Huang, S.; Chang, J.; Heo, C.; Yao, F.; Adhikari, S.; Gunes, F.; Liu, L.C.; Lee, T.H.; Oh, E.S.; et al. ZnO Nanowire Arrays on 3D Hierarchical Graphene Foam: Biomarker Detection of Parkinson's Disease. *ACS Nano* **2014**, *8*, 1639–1646. [[CrossRef](#)]
14. Haldavnekar, R.; Venkatakrishnan, K.; Tan, B. Non plasmonic semiconductor quantum SERS probe as a pathway for in vitro cancer detection. *Nat. Commun.* **2018**, *9*, 3065. [[CrossRef](#)]
15. Bu, Y.; Chen, Z.; Li, W.; Hou, B. Highly Efficient Photocatalytic Performance of Graphene–ZnO Quasi-Shell–Core Composite Material. *ACS Appl. Mater. Interfaces* **2013**, *5*, 12361–12368. [[CrossRef](#)]
16. Ezeigwe, E.R.; Tan, M.T.T.; Khiew, P.S.; Siong, C.W. One-step green synthesis of graphene/ZnO nanocomposites for electrochemical capacitors. *Ceram. Int.* **2015**, *41*, 715–724. [[CrossRef](#)]
17. Bera, S.; Pal, M.; Naskar, A.; Jana, S. Hierarchically structured ZnO-graphene hollow microspheres towards effective reusable adsorbent for organic pollutant via photodegradation process. *J. Alloy. Compd.* **2016**, *669*, 177–186. [[CrossRef](#)]
18. Xu, S.; Fu, L.; Pham, T.S.H.; Yu, A.; Han, F.; Chen, L. Preparation of ZnO flower/reduced graphene oxide composite with enhanced photocatalytic performance under sunlight. *Ceram. Int.* **2015**, *41*, 4007–4013. [[CrossRef](#)]
19. Han, C.; Chen, Z.; Zhang, N.; Colmenares, J.C.; Xu, Y.-J. Hierarchically CdS Decorated 1D ZnO Nanorods-2D Graphene Hybrids: Low Temperature Synthesis and Enhanced Photocatalytic Performance. *Adv. Funct. Mater.* **2015**, *25*, 221–229. [[CrossRef](#)]
20. Li, W.; Fang, X.; Wang, D.; Tian, F.; Wang, H.; Fang, D.; Li, J.; Chu, X.; Zhao, H.; Wang, D.; et al. Band and optical properties of arsenene and antimonene lateral heterostructure by first-principles calculations. *Phys. E Low-Dimens. Syst. Nanostructures* **2021**, *134*, 114933. [[CrossRef](#)]
21. Tian, F.; Wang, D.; Tan, F.; Fang, X.; Li, W.; Wang, H.; Wang, D.; Zhao, H.; Fang, D.; Wei, Z.; et al. Strain-Dependent Band Structures and Electronic Properties in Sb/Bi Lateral Heterostructures Calculated by First Principles. *Phys. Status Solidi –Rapid Res. Lett.* **2021**, *15*, 2100148. [[CrossRef](#)]
22. Wang, D.; Wang, F.; Wang, Y.; Fan, Y.; Zhao, B.; Zhao, D. Interfacial Emission Adjustment in ZnO Quantum Dots/p-GaN Heterojunction Light-Emitting Diodes. *J. Phys. Chem. C* **2015**, *119*, 2798–2803. [[CrossRef](#)]
23. Wang, Y.; Fang, X.; Li, R.; Li, Y.; Yao, B.; Wang, D.; Tang, J.; Fang, D.; Wang, X.; Wang, X.; et al. Surface sulfurization of ZnO/ZnS core shell nanowires and shell layers dependent optical properties. *J. Mater. Sci. Mater. Electron.* **2018**, *29*, 7924–7929. [[CrossRef](#)]
24. Fang, X.; Wei, Z.; Yang, Y.; Chen, R.; Li, Y.; Tang, J.; Fang, D.; Jia, H.; Wang, D.; Fan, J.; et al. Ultraviolet Electroluminescence from ZnS@ZnO Core–Shell Nanowires/p-GaN Introduced by Exciton Localization. *ACS Appl. Mater. Interfaces* **2016**, *8*, 1661–1666. [[CrossRef](#)]
25. Xu, Y.; Ma, G.; Wang, G.; Shi, L.; Zhang, H.; Jin, L.; Ma, X.; Zou, Y.; Yin, J.; Li, Y. Interface State Luminescence and Sub-Bandgap Absorption Based on CuGaO₂ Nanoplates/ZnO Nanowires Heterostructure Arrays. *Phys. Status Solidi* **2018**, *255*, 1800391. [[CrossRef](#)]
26. Xu, Y.; Li, Y.; Shi, L.; Li, D.; Zhang, H.; Jin, L.; Xu, L.; Ma, X.; Zou, Y.; Yin, J. Reverse-bias-driven whispering gallery mode lasing from individual ZnO microwire/p-Si heterojunction. *Nanoscale* **2018**, *10*, 5302–5308. [[CrossRef](#)] [[PubMed](#)]

27. Kumar, S.; Sharma, V.; Bhattacharyya, K.; Krishnan, V. N-doped ZnO–MoS₂ binary heterojunctions: The dual role of 2D MoS₂ in the enhancement of photostability and photocatalytic activity under visible light irradiation for tetracycline degradation. *Mater. Chem. Front.* **2017**, *1*, 1093–1106. [[CrossRef](#)]
28. Kudo, A.; Miseki, Y. Heterogeneous photocatalyst materials for water splitting. *Chem. Soc. Rev.* **2009**, *38*, 253–278. [[CrossRef](#)] [[PubMed](#)]
29. Allen, M.J.; Tung, V.C.; Kaner, R.B. Honeycomb Carbon: A Review of Graphene. *Chem. Rev.* **2010**, *110*, 132–145. [[CrossRef](#)]
30. Luan, V.H.; Tien, H.N.; Hur, S.H. Fabrication of 3D structured ZnO nanorod/reduced graphene oxide hydrogels and their use for photo-enhanced organic dye removal. *J. Colloid Interface Sci.* **2015**, *437*, 181–186. [[CrossRef](#)]
31. Song, C.; Yin, X.; Han, M.; Li, X.; Hou, Z.; Zhang, L.; Cheng, L. Three-dimensional reduced graphene oxide foam modified with ZnO nanowires for enhanced microwave absorption properties. *Carbon* **2017**, *116*, 50–58. [[CrossRef](#)]
32. Kumar, S.; Dhiman, A.; Sudhagar, P.; Krishnan, V. ZnO-graphene quantum dots heterojunctions for natural sunlight-driven photocatalytic environmental remediation. *Appl. Surf. Sci.* **2018**, *447*, 802–815. [[CrossRef](#)]
33. Soci, C.; Zhang, A.; Xiang, B.; Dayeh, S.A.; Aplin, D.P.R.; Park, J.; Bao, X.Y.; Lo, Y.H.; Wang, D. ZnO Nanowire UV Photodetectors with High Internal Gain. *Nano Lett.* **2007**, *7*, 1003–1009. [[CrossRef](#)] [[PubMed](#)]
34. Charipar, K.; Kim, H.; Piqué, A.; Charipar, N. ZnO Nanoparticle/Graphene Hybrid Photodetectors via Laser Fragmentation in Liquid. *Nanomaterials* **2020**, *10*, 1648. [[CrossRef](#)] [[PubMed](#)]
35. Wang, J.; Li, Y.; Ge, J.; Zhang, B.-P.; Wan, W. Improving photocatalytic performance of ZnO via synergistic effects of Ag nanoparticles and graphene quantum dots. *Phys. Chem. Chem. Phys.* **2015**, *17*, 18645–18652. [[CrossRef](#)] [[PubMed](#)]
36. Zeng, Z.; Wang, D.; Wang, J.; Jiao, S.; Liu, D.; Zhang, B.; Zhao, C.; Liu, Y.; Liu, Y.; Xu, Z.; et al. Broadband Detection Based on 2D Bi₂Se₃/ZnO Nanowire Heterojunction. *Crystals* **2021**, *11*, 169. [[CrossRef](#)]
37. Dhar, S.; Majumder, T.; Mondal, S.P. Graphene Quantum Dot-Sensitized ZnO Nanorod/Polymer Schottky Junction UV Detector with Superior External Quantum Efficiency, Detectivity, and Responsivity. *ACS Appl. Mater. Interfaces* **2016**, *8*, 31822–31831. [[CrossRef](#)] [[PubMed](#)]
38. Ebrahimi, M.; Samadi, M.; Yousefzadeh, S.; Soltani, M.; Rahimi, A.; Chou, T.-C.; Chen, L.-C.; Chen, K.-H.; Moshfegh, A.Z. Improved Solar-Driven Photocatalytic Activity of Hybrid Graphene Quantum Dots/ZnO Nanowires: A Direct Z-Scheme Mechanism. *ACS Sustain. Chem. Eng.* **2017**, *5*, 367–375. [[CrossRef](#)]
39. Ghosh, D.; Kapri, S.; Bhattacharyya, S. Phenomenal Ultraviolet Photoresponsivity and Detectivity of Graphene Dots Immobilized on Zinc Oxide Nanorods. *ACS Appl. Mater. Interfaces* **2016**, *8*, 35496–35504. [[CrossRef](#)]
40. Khoa, N.T.; Kim, S.W.; Yoo, D.-H.; Cho, S.; Kim, E.J.; Hahn, S.H. Fabrication of Au/Graphene-Wrapped ZnO-Nanoparticle-Assembled Hollow Spheres with Effective Photoinduced Charge Transfer for Photocatalysis. *ACS Appl. Mater. Interfaces* **2015**, *7*, 3524–3531. [[CrossRef](#)]
41. Lv, T.; Pan, L.; Liu, X.; Sun, Z. Enhanced photocatalytic degradation of methylene blue by ZnO–reduced graphene oxide–carbon nanotube composites synthesized via microwave-assisted reaction. *Catal. Sci. Technol.* **2012**, *2*, 2297–2301. [[CrossRef](#)]
42. Wu, J.; Shen, X.; Jiang, L.; Wang, K.; Chen, K. Solvothermal synthesis and characterization of sandwich-like graphene/ZnO nanocomposites. *Appl. Surf. Sci.* **2010**, *256*, 2826–2830. [[CrossRef](#)]
43. Xu, Q.; Cheng, Q.; Zhong, J.; Cai, W.; Zhang, Z.; Wu, Z.; Zhang, F. A metal–semiconductor–metal detector based on ZnO nanowires grown on a graphene layer. *Nanotechnology* **2014**, *25*, 055501. [[CrossRef](#)] [[PubMed](#)]
44. Boruah, B.; Mukherjee, A.; Misra, A. Sandwiched assembly of ZnO nanowires between graphene layers for a self-powered and fast responsive ultraviolet photodetector. *Nanotechnology* **2016**, *27*, 095205. [[CrossRef](#)] [[PubMed](#)]
45. Roy, P.; Periasamy, A.P.; Liang, C.-T.; Chang, H.-T. Synthesis of Graphene-ZnO-Au Nanocomposites for Efficient Photocatalytic Reduction of Nitrobenzene. *Environ. Sci. Technol.* **2013**, *47*, 6688–6695. [[CrossRef](#)] [[PubMed](#)]
46. Dou, P.; Tan, F.; Wang, W.; Sarreshteh, A.; Qiao, X.; Qiu, X.; Chen, J. One-step microwave-assisted synthesis of Ag/ZnO/graphene nanocomposites with enhanced photocatalytic activity. *J. Photochem. Photobiol. A Chem.* **2015**, *302*, 17–22. [[CrossRef](#)]
47. Li, Z.; Ye, L.; Lei, F.; Wang, Y.; Xu, S.; Lin, S. Enhanced electro-photo synergistic catalysis of Pt (Pd)/ZnO/graphene composite for methanol oxidation under visible light irradiation. *Electrochim. Acta* **2016**, *188*, 450–460. [[CrossRef](#)]
48. Bhirud, A.; Sathaye, S.; Waichal, R.; Park, C.-J.; Kale, B. In situ preparation of N–ZnO/graphene nanocomposites: Excellent candidate as a photocatalyst for enhanced solar hydrogen generation and high performance supercapacitor electrode. *J. Mater. Chem. A* **2015**, *3*, 17050–17063. [[CrossRef](#)]
49. Tayyebi, A.; outokesh, M.; Tayebi, M.; Shafikhani, A.; Şengör, S.S. ZnO quantum dots-graphene composites: Formation mechanism and enhanced photocatalytic activity for degradation of methyl orange dye. *J. Alloy. Compd.* **2016**, *663*, 738–749. [[CrossRef](#)]
50. Boruah, B.D.; Mukherjee, A.; Sridhar, S.; Misra, A. Highly Dense ZnO Nanowires Grown on Graphene Foam for Ultraviolet Photodetection. *ACS Appl. Mater. Interfaces* **2015**, *7*, 10606–10611. [[CrossRef](#)]
51. Shao, D.; Gao, J.; Xin, G.; Wang, Y.; Li, L.; Shi, J.; Lian, J.; Koratkar, N.; Sawyer, S. Cl-Doped ZnO Nanowire Arrays on 3D Graphene Foam with Highly Efficient Field Emission and Photocatalytic Properties. *Small* **2015**, *11*, 4785–4792. [[CrossRef](#)]
52. Cai, R.; Wu, J.-G.; Sun, L.; Liu, Y.-J.; Fang, T.; Zhu, S.; Li, S.-Y.; Wang, Y.; Guo, L.-F.; Zhao, C.-E.; et al. 3D graphene/ZnO composite with enhanced photocatalytic activity. *Mater. Des.* **2016**, *90*, 839–844. [[CrossRef](#)]
53. Men, X.; Chen, H.; Chang, K.; Fang, X.; Wu, C.; Qin, W.; Yin, S. Three-dimensional free-standing ZnO/graphene composite foam for photocurrent generation and photocatalytic activity. *Appl. Catal. B Environ.* **2016**, *187*, 367–374. [[CrossRef](#)]

54. Zhang, C.; Zhang, J.; Su, Y.; Xu, M.; Yang, Z.; Zhang, Y. ZnO nanowire/reduced graphene oxide nanocomposites for significantly enhanced photocatalytic degradation of Rhodamine 6G. *Phys. E Low-Dimens. Syst. Nanostruct.* **2014**, *56*, 251–255. [[CrossRef](#)]
55. Moussa, H.; Girot, E.; Mozet, K.; Alem, H.; Medjahdi, G.; Schneider, R. ZnO rods/reduced graphene oxide composites prepared via a solvothermal reaction for efficient sunlight-driven photocatalysis. *Appl. Catal. B Environ.* **2016**, *185*, 11–21. [[CrossRef](#)]
56. Bai, X.; Sun, C.; Liu, D.; Luo, X.; Li, D.; Wang, J.; Wang, N.; Chang, X.; Zong, R.; Zhu, Y. Photocatalytic degradation of deoxynivalenol using graphene/ZnO hybrids in aqueous suspension. *Appl. Catal. B: Environ.* **2017**, *204*, 11–20. [[CrossRef](#)]
57. Pawar, R.C.; Lee, C.S. Single-step sensitization of reduced graphene oxide sheets and CdS nanoparticles on ZnO nanorods as visible-light photocatalysts. *Appl. Catal. B Environ.* **2014**, *144*, 57–65. [[CrossRef](#)]
58. Gong, M.; Liu, Q.; Cook, B.; Kattel, B.; Wang, T.; Chan, W.-L.; Ewing, D.; Casper, M.; Stramel, A.; Wu, J.Z. All-Printable ZnO Quantum Dots/Graphene van der Waals Heterostructures for Ultrasensitive Detection of Ultraviolet Light. *ACS Nano* **2017**, *11*, 4114–4123. [[CrossRef](#)] [[PubMed](#)]
59. Cook, B.; Liu, Q.; Liu, J.; Gong, M.; Ewing, D.; Casper, M.; Stramel, A.; Wu, J. Facile zinc oxide nanowire growth on graphene via a hydrothermal floating method: Towards Debye length radius nanowires for ultraviolet photodetection. *J. Mater. Chem. C* **2017**, *5*, 10087–10093. [[CrossRef](#)]
60. Liu, S.; Liao, Q.; Lu, S.; Zhang, Z.; Zhang, G.; Zhang, Y. Strain Modulation in Graphene/ZnO Nanorod Film Schottky Junction for Enhanced Photosensing Performance. *Adv. Funct. Mater.* **2016**, *26*, 1347–1353. [[CrossRef](#)]
61. Tang, R.; Han, S.; Teng, F.; Hu, K.; Zhang, Z.; Hu, M.; Fang, X. Size-Controlled Graphene Nanodot Arrays/ZnO Hybrids for High-Performance UV Photodetectors. *Adv. Sci.* **2018**, *5*, 1700334. [[CrossRef](#)] [[PubMed](#)]
62. Liu, H.; Sun, Q.; Xing, J.; Zheng, Z.; Zhang, Z.; Lü, Z.; Zhao, K. Fast and Enhanced Broadband Photoresponse of a ZnO Nanowire Array/Reduced Graphene Oxide Film Hybrid Photodetector from the Visible to the Near-Infrared Range. *ACS Appl. Mater. Interfaces* **2015**, *7*, 6645–6651. [[CrossRef](#)] [[PubMed](#)]